Prox-1 Attitude Determination and Control

Amanda N. Pietruszewski
Prox-1 Attitude Determination and Control Subsystem Lead
gth694e@mail.gatech.edu

David A. Spencer
Research Advisor, Prox-1 Principal Investigator
david.spencer@aerospace.gatech.edu

Institute: Georgia Institute of Technology
Department: Daniel Guggenheim School of Aerospace Engineering
Laboratory: Center for Space Systems
Course: AE 8900, Special Problems Course

Abstract

The Prox-1 mission is Georgia Institute of Technology's entry to the University Nanosat Program's competition cycle. Since the goal of the program is to design a complete satellite that will function on orbit, it must have fully designed and space capable subsystems. This paper details the design of the Attitude Determination and Control Subsystem. First, the requirements for the subsystem are derived from the mission requirements, and then trades are presented to find which architecture is the best selection to meet these requirements. Then the trades for specific hardware selections are done, followed by the hardware budgets and tests. Once the hardware is chosen, the algorithms can be explored and described. A rough analysis of detumble length is done, followed be a detailed derivation and explanation of the coarse attitude control system. A filter for attitude determination is explained, followed by a discussion of the fine attitude determination and control system and then the flight rules for the system. Thus, the design of the system done to date is presented in this paper.

Table of Contents

Table of Figures

Table of Tables

Nomenclature

°	=	degrees (unit)
A	=	Amperes (unit)
ADCS	=	Attitude Determination and Control Subsystem
AFRL	=	Air Force Research Laboratory
CMG	=	Control Moment Gyro
DOF	=	Degree of Freedom
ECEF	=	Earth-Centered, Earth-Fixed coordinate frame
EME J2000	=	Earth-Centered Inertial, Earth Mean Equator January, 2000 coordinate frame
FOV	=	Field of View
G	=	Gauss (unit)
I&T	=	Integration and Test
i.e.	=	that is
km	=	kilometer (unit)
LEO	=	Low Earth Orbit
LVLH	=	Local-Vertical, Local-Horizontal Frame
m	=	meter (unit)
N	=	Newton (unit)
NS-6	=	sixth competition cycle of UNP
NS-7	=	seventh competition cycle of UNP
R^3	=	Rapid Reconnaissance and Response
RVM	=	Requirements Verification Matrix
UNP	=	University Nanosat Program
VF-ST	=	Valley Forge Star Tracker

I. Introduction

THE Prox-1 mission is a satellite mission which endeavors to use artificial potential functions for proximity operations as a means of autonomous safe trajectory control. The mission is comprised of two satellites: a microsat, called henceforth the Prox-1 satellite, and a CubeSat. The Prox-1 satellite shall eject the CubeSat with the desire to rendezvous with it and then circumnavigate it. When within sensor range of the CubeSat, the Prox-1 satellite will use image-based observations for navigation and closed-loop attitude control relative to the CubeSat.

It is important to note that the Prox-1 satellite is being developed by Georgia Institute of Technology as a part of the University Nanosat Program's (UNP) seventh competition cycle (NS-7). UNP is a program run by the Air Force Research Laboratory (AFRL), which funds schools during a two year competition cycle to design militarily relevant satellite missions. At the end of the two year mission, one of the schools is selected for a launch opportunity. Because this competition seeks to put a satellite in space, it is important that all subsystem designs not be simply academic but be rigorously designed and tested to space quality.

The Attitude Determination and Control Subsystem (ADCS) is one of the subsystems of the Prox-1 mission and the focus of this paper. The ADCS has two primary responsibilities: determining the orientation of the spacecraft with respect to the Earth or other reference frames, and positioning the spacecraft in a desired orientation. Though some scientific mission can be accomplished with very little pointing knowledge or in free tumble, the mission of the Prox-1 satellite cannot. The Prox-1satellite must be able to determine where it is on its orbit so that it knows where it is relative to the CubeSat. It must also know which direction it is pointing and be able to change that pointing, so it can point its imagers at the CubeSat.

This paper will develop the design for the Prox-1 satellite's ADCS. It will first show how the requirements for the subsystem are found, flowing down the subsystem requirements from the mission statement and other high level requirements.

After understanding the requirements, an ADCS architecture will be selected, where an architecture is comprised of different types of hardware and software to make a working ADCS system. Trade studies of different combinations will be explored and one will be selected. The next section will then explore the consequences of the hardware architecture in detail. Trade studies will be presented that will determine what specific piece of hardware will be chosen, and some of the tests for the hardware will be presented.

The following chapter will explore the software and algorithms that are needed for the selected architecture. A coarse control law algorithm will be developed as well as a basic filter for attitude determination. An initial design of the fine ADCS system will be discussed as well. The section will be closed with a discussion of the flight rules required for both fine and coarse systems.

The paper will be closed with a brief conclusion. Important, pertinent memos written during the design process will be presented in the Appendix.

II. Requirements

All of the requirements for the Prox-1 mission are contained within the Requirements Verification Matrix (RVM). This matrix starts with the mission statement and from that statement, derives requirements for the mission, systems, and subsystems, including ADCS. Table I contains the ADCS requirements as well as the higher level requirements from which the ADCS requirements flow down. These higher level requirements are included to show good systems engineering, i.e. the ADCS requirements were created for the reason of enabling the main mission of the satellite.

It is important to note that these requirements were valid as of the time this paper was written. Requirements are subject to change as the mission evolves until the requirements are frozen.

Table I ADCS Requirements Flow Down

Number	Requirement	Source
	Mission Objectives	
MO-1	Prox-1 shall deploy a target CubeSat.	
MO-2	Prox-1 shall use low thrust propulsion for rendezvous and circumnavigation of the CubeSat.	
MO-3	Prox-1 shall use artificial potential functions for autonomous safe trajectory control.	
MO-4	Prox-1 shall use image based observations for relative navigation and closed-loop attitude control.	
	Mission Success Critera	
MSC-1	Prox-1 shall deploy a target CubeSat.	MO-1
MSC-2	Prox-1 shall rendezvous with the target	MO-1,MO-2
MSC-3	Prox-1 shall circumnavigate the target	MO-1,MO-2
MSC-4	Prox-1 shall use low thrust propulsion for rendezvous and circumnavigation of the CubeSat.	MO-1,MO-2
MSC-5	Prox-1 shall acquire thermal images of the target.	MO-3,MO-4,
MSC-6	Prox-1 shall acquire visible images of the target.	MO-3,MO-4,
MSC-7	Prox-1 shall navigate and perform attitude control based upon acquired images using onboard processes.	MO-3,MO-4,
	Mission Design	
MD-1	The duration of the primary mission shall be one month.	MSC-1, MSC-2, MSC-3, MSC-4, MSC-5, MSC-6, MSC-7
MD-3	Prox-1 shall perform proximity operations within a range of 50 m and 200 m of the CubeSat.	MSC-1, MSC-2, MSC-3, MSC-4, MSC-5, MSC-6
	Space Systems	
SS-2	The Prox-1 satellite and CubeSat shall be designed to withstand the launch and the environment of the launch vehicle without failure, leaking hazardous fluids, or releasing anything that could damage the LV or cause injury to the ground handling crew.	NUG
SS-3	The Prox-1 satellite and all components, including CubeSat, shall be capable of surviving operation in space for the primary mission duration.	MD-1

Science Instruments		
INS-1	The Prox-1 satellite shall use a microbolometer thermal imager to acquire thermal images of the target.	MSC-5
INS-1.3	The microbolometer thermal imager shall be protected from incident solar radiation.	SS-3
INS-1.3.1	The microbolometer thermal imager pointing vector shall be maintained at no less than ten degrees from the solar vector.	SS-3, INS-1.3
INS-2	A camera baffle shall be integrated onto the visible camera to protect the microbolometer thermal imager from stray light.	SS-3, INS-1.3
INS-2.3	The Prox-1 satellite shall use a visible camera to acquire visible images of the target.	MSC-6
INS-2.3.1	The visible camera shall be protected from incident solar radiation.	SS-3
Communications Subsystem		
COM-1	The COM Subsytem shall provide uplink and downlink communications between the Prox-1 satellite and the Georgia Tech Ground Station, or other authorized ground stations.	MSC-5, MSC-6
COM-1.6	The COM Subsystem shall maintain a link margin of at least 3 dB for communications with the Ground Station.	COM-1
Attitude Determination and Control Subsystem		
ADC-1	The Prox-1 satellite shall be three-axis stabilized.	MSC-2, MSC-3, MSC-4, MSC-5, MSC-6
ADC-2	The ADCS shall damp attitude rates to less than [0.5] deg/s within 3 hours of launch vehicle separation.	SS-2,MD-3
ADC-3	The ADCS shall be capable of coarse attitude control within [40] degrees per axis.	COM-1.6
ADC-3.1	The ADCS shall use torque rods for coarse attitude control.	ADC-3
ADC-3.2	The ADCS shall acquire coarse attitude determination within [20] degrees per axis.	ADC-3
ADC-3.2.1	The ADCS shall use a magnetometer for coarse attitude determination.	ADC-3.2
ADC-3.2.2	The ADCS shall acquire orbit position knowledge at a frequency of 0.5 Hz at an accuracy of 15 m.	ADC-3.2
ADC-3.2.2.1	The ADCS shall use a GPS unit for orbit position knowledge.	ADC-3.2.2
ADC-3.2.3	The ADCS shall acquire orbit velocity knowledge at a frequency of 0.5 Hz at an accuracy of 0.25 m/s.	ADC-3.2
ADC-3.2.3.1	The ADCS shall use a GPS unit for orbit velocity knowledge.	ADC-3.2.3
ADC-4	The ADCS shall be capable of fine attitude control within [3.0] degrees per axis.	MSC-5, MSC-6
ADC-4.1	The ADCS shall use reaction wheels for fine attitude control.	ADC-4
ADC-4.2	The ADCS shall acquire fine attitude determination within [0.5] deg per axis.	ADC-4
ADC-4.2.1	The ADCS shall use a star tracker for fine attitude determination.	ADC-4.2
ADC-4.2.2	The ADCS shall use the thermal and visible images to determine the unit vector from the Prox-1 satellite to the CubeSat.	MSC-7, ADC-4.2
ADC-5	The Prox-1 satellite shall maintain a Sun exclusion zone of [+/- 15 degrees] for the microbolometer and visible camera.	INS-1.3.1, INS-2.3.1
ADC-5.1	The AODCS shall use one sun sensor to monitor sun position relative to imaging instruments.	ADC-5

III. Subsystem Architecture

As is the case for many subsystems, an attitude determination and control subsystem cannot simply be determined by picking hardware and then the appropriate software. The architecture of the entire subsystem must be taken into account. Different combinations of hardware dictate different software, such that a system with only a magnetometer versus a system with a magnetometer and sun sensors create vastly different system architectures. Therefore, first architectures as a whole must be considered, where an architecture consists of different combinations of hardware and software to make a complete attitude determination and control subsystem.

Two types of architectures will be discussed here: a fine ADCS and a coarse ADCS. Fine ADCS is the more accurate system to be used during science modes of the spacecraft. Coarse ADCS is the less accurate, lower power system to be used during safe and low power modes.

First, the fine ADCS architecture will be discussed, since its need is derived from the payload requirements. However, from the discussion of this subsystem, it will be clear that a coarse ADCS architecture that is separate from (though at times overlapping) the fine ADCS will also need to be developed; therefore, the discussion of the coarse ADCS will be discussed.

A. Fine ADCS Architecture

1. Fine Attitude Control Architecture

It might seem an impossible task to determine an architecture, given that there are so many possibilities and variants. However, looking at the requirements for the system, it is obvious that some architectures can be discarded out of hand. The system is not nadir-pointing, but rather must point towards the CubeSat; therefore, a gravity gradient system is not acceptable. The system also requires three-axis control. A spin-stabilized spacecraft would not be able to meet this requirement. Only control systems that control all three axes and can maneuver to different attitudes, such as nadir-pointing, sun-pointing, CubeSat-pointing, and other commanded attitudes, can be considered.

This leads to the consideration of four different types of control systems: propulsion, torque rods, control moment gyros (CMG), and reaction wheels.

Many trades taken into account in this paper will consider the heritage design from the Rapid Reconnaissance and Response (R^3) mission, which was the spacecraft for the NS-6 competition cycle. In the R^3

mission, propulsion as a means of attitude control was not selected, because of the low lifetime, high mass and volume, high risk, and required waiver process. Though all of these factors are still important and true for the Prox-1 mission, it should be noted that the Prox-1 mission will have propulsion. A propulsion subsystem is necessary in order to rendezvous with and circumnavigate the CubeSat. Because the propulsion system is already required, using this system for ADCS must be seriously considered.

At the time of this paper, an electric propulsion system was still the baseline design of the propulsion subsystem. However, a serious trade study is currently being performed to replace the electric propulsion system with a cold gas system. Here both architecture variants will be discussed, and it will be determined if propulsion is a valid means of attitude control when considering either architecture.

First, the electric propulsion system shall be considered. The propulsion subsystem's design only requires one Hall thruster. For attitude control, one Hall thruster would not be enough since one thruster can only translate the satellite in one direction. An attitude control propulsion system would need to be able to control every axis, so that the satellite could rotate about any axis. However, the use of one Hall thruster has stretched the Prox-1 electrical power subsystem to the limits of its capability, requiring large deployable solar arrays. Additional Hall thrusters would only increase the power requirement, which the power subsystem would be unable to meet. Therefore, the use of electric propulsion for attitude control is not feasible.

However, one must explore if the switch to cold gas propulsion for circumnavigation and rendezvous would open the attitude control to the possibility of using propulsion as well. The important consideration here is the amount of propellant that the satellite can carry. The current propulsion design requires only two thrusters, to control the satellite on one axis, but as noted before, attitude control requires control around all axes. Circumnavigation and rendezvous is a tricky task that will require a large amount of propellant. Attitude control will also need a good amount of propellant since the thrusters will have to fire every time the attitude needs to be corrected. Risk must also be considered. Added thrusters are added risk, the primary concern being that if the valve fails in the open position all of the propellant would be discarded into space and the satellite would move in an undesired fashion. Also, the Prox-1 mission requires a rather steady pointing system, in order to image the CubeSat. Thrusters are a bang-bang control system, meaning they are fired when the satellite hits the pointing requirement limits but not used to continuously hold it steady at one position. All of these considerations make propulsion a poor choice for the Prox-1 mission.

It should be noted at this point that one of these propulsion systems will be used on the Prox-1 satellite for orbit control, i.e. circumnavigation and rendezvous with the CubeSat. However, since they have been determined to be unfit for attitude control, the system becomes a separate subsystem and not part of the ADCS.

The next attitude control system architecture to be considered is torque rods alone. Since both CMGs and reaction wheels require torque rods in addition to their systems for momentum dumping purposes, it makes sense to first consider this more basic system alone (Wertz, Spacecraft Attitude Determination and Control, 1978). It should be noted that torque rods, magnetoquers, magnetic torquers, and other similar names are all used synonymously to mean the same device, but for the sake of this paper, the devices shall merely be called torque rods. Torque rods are a component where the magnetic moment created by the torque rod interacts with the Earth's magnetic field in order to create a torque, i.e. the torque is equal to the cross product of the torque rod's magnetic moment with the Earth's magnetic field strength (Wertz, Spacecraft Attitude Determination and Control, 1978). This is extremely important to note because it means that any torque rod system will be under-actuated. So though a torque rod system can create a three-axis control system for long periodic motions like nadir-pointing or sun-pointing, the unperiodic motion of circumnavigation and rendezvous would be uncontrollable with a torque rod system (Psiaki, 2000). This makes torque rods alone an imperfect system for the Prox-1 mission.

A CMG is a device that creates torque by rotating about an axis, just as a reaction wheel does (Wertz, Spacecraft Attitude Determination and Control, 1978). However, CMGs have an edge over reaction wheels, since unlike reaction wheels they can gimbal about their axis (Wertz, Spacecraft Attitude Determination and Control, 1978). This is extremely efficient and allows a much finer control than reaction wheels. However, most CMGs are built for much larger spacecraft (Wertz, Spacecraft Attitude Determination and Control, 1978). There are currently no space-qualified CMGs for spacecraft in the 50 – 100 kg range. It should be noted that Cornell University's Violet mission is seeking to fill this gap in the sizing and capability of CMGs by space qualifying a set of CMGs as well as several algorithms. This will open CMGs as a control system for Prox-1 sized missions; however, because of the financial limitations of most university missions, like Prox-1, CMGs will still be out of reach for most missions.

The final system to be considered is a reaction wheel system. Reaction wheels, as previously discussed, create torque by spinning a wheel (Wertz, Spacecraft Attitude Determination and Control, 1978). This is the concept of conservation of angular momentum. When a reaction wheel spins up, it places a torque on the spacecraft structure, causing it to spin in the opposite direction in order to conserve its total angular momentum. This sort of

system does require magnetic torque rods in addition to reaction wheels, for momentum dumping purposes (Wertz, Spacecraft Attitude Determination and Control, 1978). A reaction wheel system will be able to control all three axes of the satellite and hold the satellite still enough for imaging. It will also allow the satellite to slew as it circumnavigates the CubeSat. It is the most effective and low cost system for this satellite; therefore, a reaction wheel system with an additional torque rod system for momentum dumping shall be used for the Prox-1 mission. Sizing of these reaction wheels in order to meet Prox-1 requirements will be discussed in Chapter IV Hardware of this paper, when hardware selection for the fine ADCS system is discussed.

A summary of the advantages and disadvantages of each system discussed in this section can be seen in Table II.

Table II Fine Control Architecture Trade

Control System	Advantages	Disadvantages
Hall Thrusters	• Already required system*	• Additional Mass • High Power Demand
Gold Gas Propulsions	• Already required system* • High slew rates	• Additional thrusters added • Additional Risk • Additional Propellant • Unsteady pointing
Torque Rods	• Inexpensive	• Under-actuated • Low accuracy
CMGs	• High accuracy • Steady pointing	• Expensive • Not space qualified • High Mass • Requires desaturation
Reaction Wheels	• High accuracy • Steady pointing	• Requires desaturation

*One of these propulsion systems is required, not both.

Hardware

2. Fine Attitude Determination Architecture

Attitude sensors come in many varieties: sun sensors, horizon sensors, magnetometers, star trackers, gyros, and more. However, the trade for which architecture to use for the Prox-1 mission is quite simple. For the R^3 mission it was determined that a star tracker with its fine attitude knowledge, output in the form of a quaternion, would be the perfect device for the mission and the only needed component for the fine attitude determination. Because this component is already owned and available to the Prox-1 mission by the Georgia tech Center for Space Systems, it was baselined for the Prox-1 mission.

However, there should be no concern that this part is simply being used without consideration if its meets the requirements. The star tracker has an extremely fine capability that meets the requirements of the Prox-1 mission, as will be discussed further in Chapter IV of this paper, when the specifics of the hardware is discussed.

It is true that star trackers can have a difficult time locking onto the stars and determining the attitude while slewing at high rates. Such rates might be the case while Prox-1 is circumnavigating the CubeSat as well as during detumble. However, once the satellite has locked onto the CubeSat, images will be used for determining the pointing of the satellite for the purpose of keeping the CubeSat within the Field of View (FOV) of the imager. Therefore, this instability of the star tracker during circumnavigation is not a problem for Prox-1 mission architecture. The images will instead be used.

The star tracker will be used for fine attitude determination on the Prox-1 satellite. An imager will be used for relative attitude to the CubeSat. It should be noted that the imager is not part of the algorithms developed in this paper, but will be included in the fully developed algorithms for the Prox-1 mission.

A GPS unit is also necessary for fine attitude determination, because the quaternion the star tracker outputs is in an inertial reference frame. In order to convert this quaternion to an Earth-reference quaternion, knowledge of the satellite's position about the earth is required. The GPS can supply such a position, but the output of the GPS will need to be put through a filter. Then if necessary the filter GPS position can be put into an orbit propagator so that the time of the orbit position matches the time of the star tracker measurement. It should be noted that neither the GPS filter or the conversation algorithm are developed in this paper but an orbit propagator is developed.

3. Complete Fine Architecture

The decided determination and control architectures can be combined into a full fine ADCS architecture, which can be seen in Figure 1. A star tracker and GPS are used for fine determination, where the star tracker provides a quaternion in the inertial frame. The GPS provides position and time data. This data is filtered and if necessary propagated, so that the GPS data corresponds to the same instant in time as the star tracker quaternion. The two sets of data are then used to convert the inertial quaternion into an Earth-Fixed quaternion.

The quaternion contains the attitude information for the satellite. This attitude information is compared to the desired attitude that the mission profile states the satellite should be at. The difference between the two becomes the command that is inputted into the controller. The controller then calculates the torque that needs to be supplied and sends the appropriate command to the reaction wheels. Should the reaction wheels need to be desaturated, a B-

field is inputted into the controller as well so an appropriate torque can be calculated for the torque rods. The controller then sends a command to the torque rods to desaturate the reaction wheels.

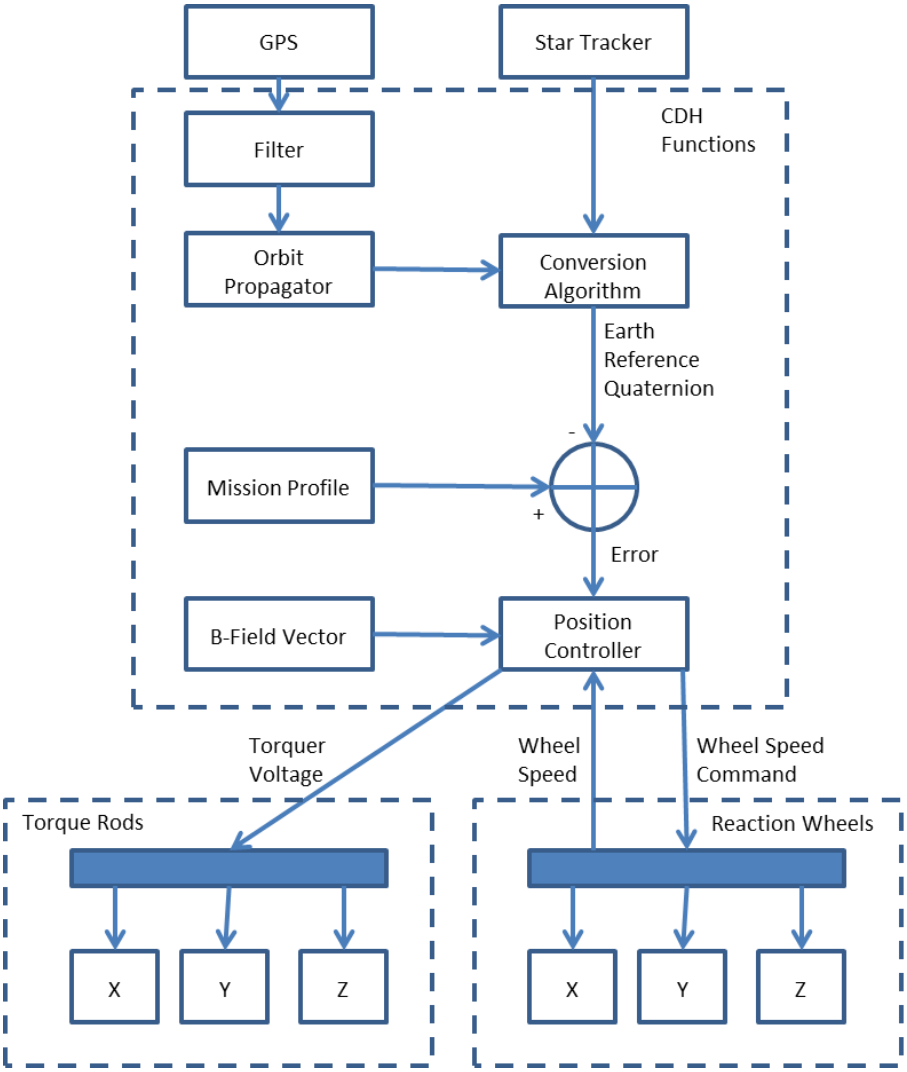

Figure 1 Fine ADCS Architecture Block Diagram

B. Coarse ADCS Architecture

Not every spacecraft mission requires two separate architectures for ADCS. However, from the requirements, a need for the previously discussed fine ADCS was derived. However, providing power for a GPS, a star tracker, reaction wheels, and torque rods is outside of the ability of low power modes, like safe mode and the initial power up of the spacecraft. Therefore, a coarse ADCS needs to be developed for these low power modes and is the primary focus of this paper.

1. Coarse Attitude Control Architecture

Determining a coarse architecture is much simpler than the trade study for the fine architecture. Our fine architecture requires a torque rod system for desaturation of the required reaction wheels. Rather than choose another system that would add mass to the spacecraft, using the torque rod system as the coarse control makes more sense.

It should be noted that any pure torque rod system is under actuated, because of the nature of how torque rods work. The magnetic moment of a torque rod crossed with the magnetic field of the Earth creates a torque. Therefore, a torque rod cannot create a torque when the axis of the torque rod is parallel to the Earth's magnetic field. However, since rotation around the Earth is a periodic system, a torque rod system can coarsely control the attitude of the satellite.

2. Coarse Attitude Determination Architecture

The use of torque rods as the mode of control requires that the Earth's magnetic field is known, so that the necessary torque can be calculated. Models could be used for this, but a magnetic field model can vary in accuracy. Some magnetic field models are as simple as a pure dipole, but there a several variables that affect the Earth's magnetic field, including the oblateness of the Earth, solar wind effects, and magnetic storms (Wertz, Spacecraft Attitude Determination and Control, 1978). Not all of these effects can be captured by a model; therefore, a way to sense the magnetic field of the Earth is required. For this, a magnetometer is the optimal instrument.

Due to these inaccuracies of the model and the electromagnetic interference caused by instruments and subsystems, magnetometers are not an optimal instrument. However, during the modes that require coarse control, only the minimal subsystems and instruments are powered on. Therefore, there is minimal interference to the magnetometer's reading. However, the torque rods do create magnetic fields when they are on that can disrupt the signal. This problem is addressed in the following section where the full architecture is discussed.

It is important to note that a magnetometer only outputs the magnetic field vector. Without much processing, this magnetic field vector can be used to determine the satellite's positional attitude (i.e. its Euler angles), but it cannot determine directly from this data the angular velocities, which are necessary to have a complete satellite attitude (Wertz, Spacecraft Attitude Determination and Control, 1978). Therefore, a filter is necessary. With the magnetometer data and a predicted magnetic field from a magnetic model, a Kalman Filter can

be used to find the full attitude of the spacecraft. This filter will be explained in detail later in the software section of this paper.

In order use a magnetic field model, the position of the satellite around the Earth must be known. Since a GPS was already required for fine determination, it is convenient to use it for coarse determination as well. This GPS will be filtered and propagated to the right moment in time, as previously described, and then the position will be inputted into a magnetic model, which will then give the predicted magnetic field. This predicted magnetic field is then inputted into the Kalman Filter, allowing the Kalman Filter to find the full attitude of the satellite.

3. Complete Coarse Architecture

The architectures for attitude determination and control are combined into a complete coarse architecture, as can be seen in Figure 2. The previously mentioned attitude determination architecture is used to find the attitude of the satellite. This attitude is then compared to the desired attitude, and this error, or commanded attitude, is inputted into the controller. The controller than determines the torque required. In order to do this, the B-Field vector must once again be accessed by the controller, since a torque rod can only produce torque based on the Earth's magnetic field. This B-Field vector is produced from the Earth Magnetic Field model mentioned earlier. The controller then sends the appropriate command to the torque rods to change the attitude as necessary.

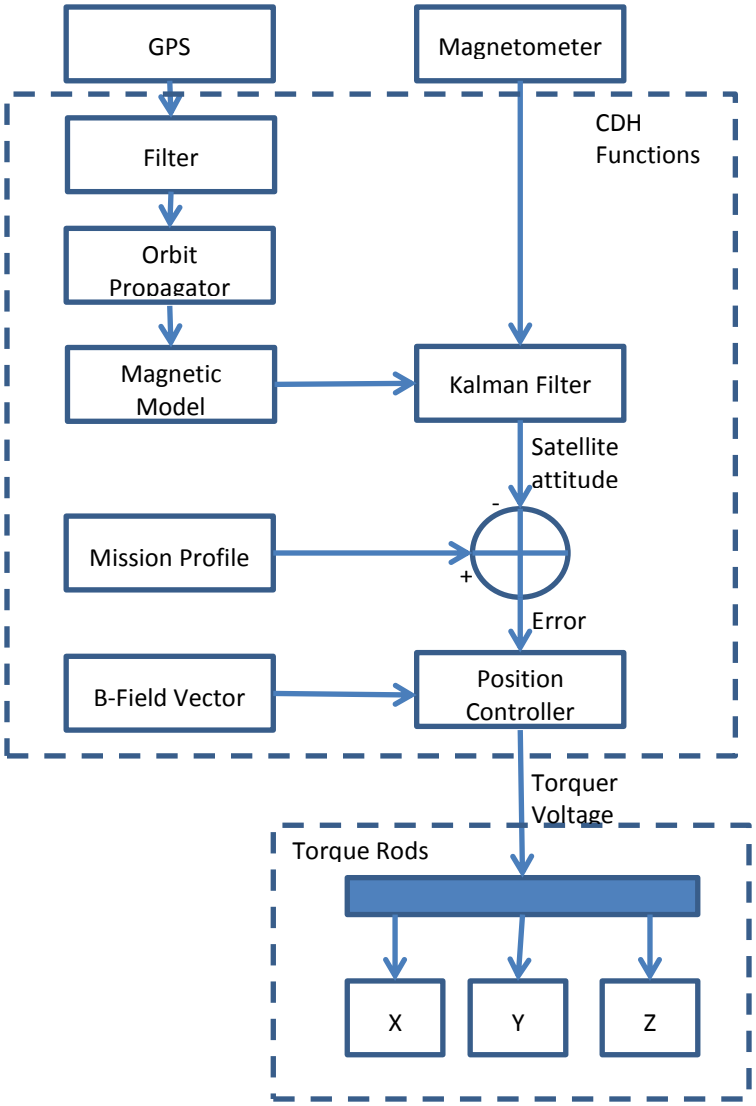

Figure 2 Coarse ADCS Architecture Block Diagram

IV. Hardware

Hardware must be discussed before software, because the design of the software is driven by the hardware selection, as will become clear in the following discussions. In this section, the selection of the hardware will be discussed, and then the mass budget and power budgets will be detailed. The final part of this section will include the Integration and Test plans created for the subsystem.

A. Hardware Selection

Hardware selection requires considering the requirements of the mission, mass and power budget restraints, and cost restraints. It should be noted that several pieces of hardware were selected during the R^3 mission but are being used for the Prox-1 mission. The original trade studies presented during the R^3 mission will be presented here, since they are the trade studies that led to the hardware selection.

1. Star Tracker Selection

Once a star tracker was chosen as the primary method of attitude determination, the particular unit had to be chosen. The units considered for the star tracker were the Galileo Avionca A-STR, the Surrey Satellite Technology Limited Altair HB+, the Terma Star Tracker HE-5AS, and the Valley Forge Star Tracker (VF-ST). The units were evaluated for size, mass, power consumption, cost, and reliability. After these considerations, it was determined that the VF-ST provides the best alternative for usage on the R^3 spacecraft. The VF-ST provides a very light, small star tracker that still performs well within the design requirements. The VF-ST also provides the cheapest alternative. The specifications of the alternative units considered can be seen in Table III.

Table III Star Tracker Alternatives

Specification	A-STR	Altair HB+	HE-5AS	VF-ST
Mass (kg)	3.0	1.66	2.2	≤ 1
Power Consumption (W)	8.9	8.5	6.8	≤ 5.0
Accuracy	10 arcsec	10 arcsec	1 arcsec	≤15 arcsec
Dimensions (mm)	195 x 175 x 288	190 x 135 x 44	245x165x29	Ø 130 x 181

The VF-ST is composed of several parts housed within a central casing. The electro-optical device used to detect individual stars is composed of Charge-Coupled Device (CCD) matrices, which create a digital signal of light stimuli. Outside of the CCD matrices is a sunshade designed to limit the amount of sunlight exposure to the device. Also within the device is a data processor that processes the digital CCD signal to recognize stars and determine the spacecraft's inertial position. It also houses the digital star catalogue used to determine the position of the spacecraft.

The specifications can be seen in Table IV , and a picture of the VF-ST can be seen in Figure 3 (S.A. Lavochkin Scientific and Production Association, 2008).

Table IV Star Tracker Specifications

Parameter	Value	Units
Mass	≤ 1	kg
Dimensions	Ø 130 x 181	mm
Power requirement	≤ 5	W
Cost	$25,000	
Time to readiness after start of power current feed	≤ 30	sec
Insulation resistance	≥ 20	MOhm
Angle of view	≥ 20^O x 15^O	
Orientation measurement error:		
$\sigma_{X,Y}$	≤ 15"	
σ_Z	≤ 70"	
Information update rate	≥ 5	Hz
Time of first definition of angular position of axes	≤ 5	sec
Number of stars in star catalogue	≥ 5000	
Maximum stellar magnitude of registered stars	≥ 6,5	
Working temperature range	-20^OC to $+50^O$C	
Voltage range	23 - 34	V
External interface port	**Rs422**	

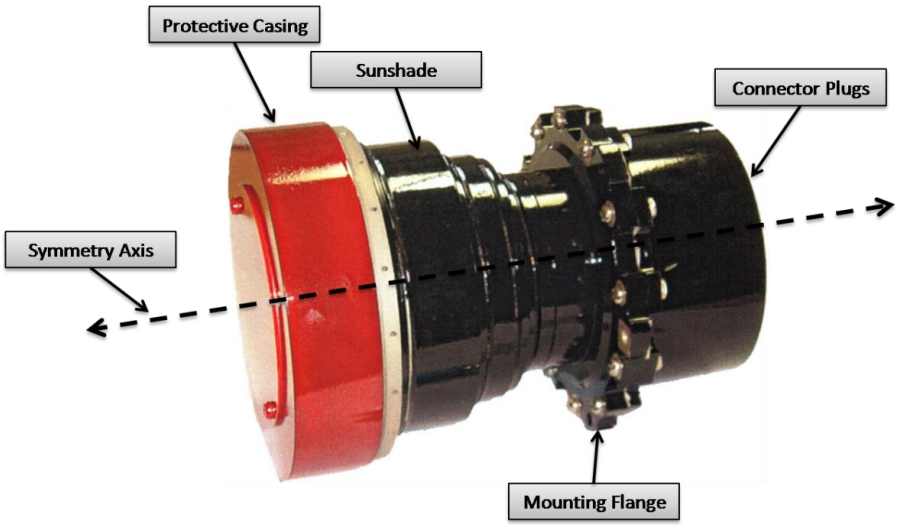

Figure 3 Valley Forge Star Tracker[1]

[1] Image Credit: (S.A. Lavochkin Scientific and Production Association, 2008)

2. GPS Selection

The orbit determination subsystem will be provided by the SpaceQuest GPS-12-VI receiver, which can be seen in Figure 4. This receiver is heavier than the originally chosen receiver and does not come with an antenna; however, the parts are traceable. The antenna that will be used is the SpaceQuest ANT-GPS, GPS flight antenna, which can be seen in Figure 5.

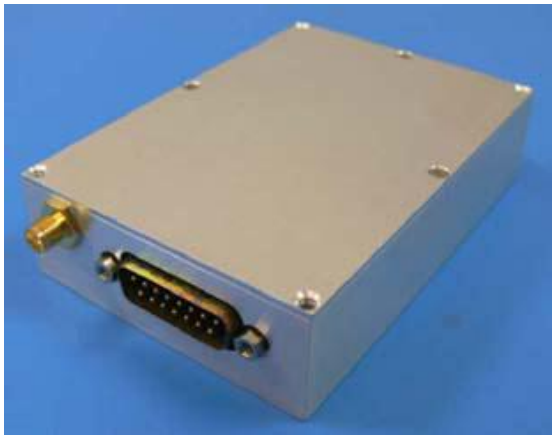

Figure 4 SpaceQuest GPS-12-V1[2]

Figure 5 SpaceQuest ANT-GPS[3]

The specifications for the GPS receiver can be seen in Table V, and the specifications for the antenna can be seen in Table VI (SpaceQuest, Ltd.).

[2] Image Credit: (SpaceQuest, Ltd.)
[3] Image Credit: (SpaceQuest, Ltd.)

Table V SpaceQuest GPS-12-V1 Specifications

Parameter	Value	Unit
Mass	< 200	g
Required Power	< 1.0	W
Dimensions	100 x 70 x 50	mm
Time Accuracy	1	μs
Position Accuracy (2σ)	10	m
Velocity Accuracy (2σ)	0.03	m/s
Time to First Fix (Cold Start)	60	sec

Table VI SpaceQuest ANT-GPS Specifications

Parameter	Value	Unit
Mass	82	g
Required Power	< 1.0	W
Dimensions	Ø52.8 x 17.5	mm
Frequency	L1, 1575.42 ± 12	MHz

The GPS unit outputs the spacecraft's position, velocity, and the Coordinated Universal Time (UTC). The position and velocity are critical to the inertial-to-Earth reference conversion of the attitude quaternion, and the UTC time output is crucial for mission operations.

3. Magnetometer Selection

A fluxgate magnetometer is baselined for the mission in order to provide secondary attitude determination as well as characterize the magnetic field for the operation of the magnetic torquers. Fluxgate magnetometers are often developed specifically for missions, but they are also available commercially; therefore, the particular commercial unit needed to be determined.

Billingsley Aerospace & Defense manufactures a small triaxial fluxgate magnetometer called the TFM65-VQS. SpaceQuest offers the Mag-3, fluxgate magnetometer. Macintyre Electronic Design Associates (MEDA), Inc. offers two fluxgate magnetometers, the TAM-1 and the TAM-2. Table VII compares the specifications of the four magnetometers.

Table VII Magnetometer Specifications

Parameter	TFM65-VQS	Mag-3	TAM-1	TAM-2
Mass	117 g	100 g	310 g	500 g
Size	3.51 x 3.23 x 8.26 cm	3.51 x 3.23 x 8.6 cm	4.76 x 6.68 x 11.9 cm	4.45 x 14.3 x 7.62 cm
Field Range	±0.6 Gauss	±1 Gauss	±1 Gauss	±1 Gauss
Input Voltage	28 VDC	15 to 34 VDC	21 to 36 VDC	21 to 38.6 VDC

For a mass and volume constrained mission like Prox-1, these become the most important requirements. It is easy to see that the SpaceQuest Mag-3 has both the lightest mass and volume (SpaceQuest, Ltd.). Therefore, the Mag-3 was chosen as the fluxgate magnetometer for the Prox-1 mission.

4. Torque Rod Selection

As explained in the Subsystem Architecture section of this paper, magnetic torquers are needed both to desaturate the reaction wheels and for coarse attitude control. To size these torquers, a calculation based on disturbance torques and the Earth's magnetic field was used (Wertz & Larson, Space Mission Analysis and Design, 1999). It revealed that the magnetic torquers would need to provide a magnetic dipole of approximately 4 Am^2. For the sake of margin, this dipole moment was increased to 10 Am^2.

To produce the magnetic moment, two types of magnetic torquers were considered: magnetic coils and torque rods. Magnetic coils are large diameter coils of wire that utilize the internal area as the primary driver of the magnetic moment. This device has the benefit of requiring few turns of wire; however, these coils are of large diameter and circumference. A magnetic torque rod is a device with a small diameter and long length wound around a central core made of magnetic material. This device uses the magnetic amplification properties of the core material to drive the magnetic moment.

For the level of magnetic moment needed by the R^3 spacecraft, magnetic coils become prohibitive in their mass and size. In the case of our 10 Am^2, the diameter of the coil would need to be nearly 70 centimeters, which is larger than the spacecraft, to supply the dipole moment. A torque rod of the same mass would remain within a two-centimeter diameter and 20 centimeter length. For this reason, a set of torque rods has been chosen as the method of magnetic torque control.

Initially, a commercial off-the-shelf torque rod was considered. However, due to the simplicity of the device, it was decided that the torque rod would be developed and built in house. This design would be based off of

the previously considered commercial model, the Microcosm Inc. MT0-2-H. This model would serve as the design basis of the specifications as shown in Table VIII.

Table VIII Magnetic Torque Rod Design Specification

Magnetic Torquer Design Goals		
Dipole Moment	10	Am^2
Mass	0.35	kg
Length	330	mm
Diameter	17	mm
Power	1	W

Design of the torque rod was not done by the author of this paper, but rather by one of the undergraduate students on the team; therefore, the design memo is presented in the appendix. However, the final results are presented here.

The material for the core of the rod was decided to be Hiperco 50a, and the dimensions are a diameter of 0.5 inches and a length of 12 inches. 30 gauge copper wire that was wrapped around the core approximately 8,500 times to create 8 layers. Details on the construction of the torque rods can be found in the appendix. After construction, actual mass of the toque rod was found to be 500 kg rather than the 350 kg initially desired. However, this mass falls well into the mass allowances of the Prox-1 system.

5. Reaction Wheel Selection

Unfortunately, sometimes selection of a component does not come as easily as was detailed in the previous studies. For the R^3 mission, a reaction wheel was selected, but due to conflict with the vendor, it was decided that a new reaction wheel needed to be chosen. However, the analysis done to select the appropriate size of the reaction wheel is still valid. Therefore, the sizing analysis will be presented here.

The sizing of the reaction wheels for the satellite was based upon a calculation of the disturbance torques on the spacecraft and the desired pointing abilities. First, a calculation of the major disturbance torques was undertaken. In this, disturbance torques were calculated for gravity gradient torques, solar radiation pressure, magnetic field torques, and aerodynamic drag forces. The worst-case estimates for the torques can be seen in Table IX.

Table IX Worst-Case Estimated Disturbance Torques

Disturbance	Torque	Units
Gravity Gradient	0.4304	μN*m
Solar Radiation	0.4374	μN*m
Magnetic Field	50.0077	μN*m
Aerodynamics	15.8053	μN*m

As it is clear to see, these disturbance torques are very small, and thus the required torque from a reaction wheel to reject them is not very significant. Therefore, the main criterion considered for the sizing of the reaction wheels was the slewing requirement for pointing. A slewing requirement of 5 deg/s was listed in the original R^3 proposal, but this requirement was not based upon any design constraint. When reevaluated, this requirement was far too stringent for the requirements of the system. For a pointing zone of ±15°, the maximum attitude change of 30° could be achieved in approximately six seconds. The R^3 mission does not require this level of maneuverability and thus the slew rate requirement was relaxed. It is likely that the minimum time the satellite required to move to a position would be one minute. This corresponds to a slew rate of 0.5 deg/s, a much more reasonable slewing requirement. Using this requirement, it is possible to calculate the size of the reaction wheels necessary to achieve this slew rate. Also, it is possible to roughly estimate the minimum momentum required for a reaction wheel to reject a disturbance throughout a complete orbit. The maximum worst-case disturbance torque, the magnetic field torque, is used to evaluate this. The resulting parameters can be seen in Table X.

Table X Minimum Specifications for Reaction Wheels

Parameter	Value	Unit
Torque Required for Disturbance Rejection	100.0153	μN*m
Torque Required for Slew Rate	2.9574	mN*m
Momentum Required for Disturbance Rejection	0.0502	N*m*s

Using this specification, it is possible to determine the appropriate size needed for reaction wheels. Adding margin, it was decided that reaction wheels that can provide a momentum of 0.1 Nms would be ideal for the R^3 satellite. This analysis still holds true for the Prox-1 mission, since the two satellites are of the same size and have extremely similar pointing requirements.

6. Sun Sensor Selection

Though for pure attitude determination and control, the satellite does not require sun sensors, the imagers necessary to meet the mission requirements of the Prox-1 mission cannot survive exposure to the sun. Solar panels can generally be used as extremely coarse sun sensors, to determine where the sun is when necessary. However, the imagers have a strict sun exclusion angle of 10 degrees (INS-1.3.1). Fortunately, both of the imagers are on the nadir face; therefore, only one sun sensor is necessary for the Prox-1 mission. The sun sensor can be placed on the nadir face and monitor the sun angle to this face and subsequently the imagers.

Several sun sensors were considered, but most were too costly. The AeroAstro coarse sun sensor was chosen and can be seen in Figure 6 and the specifications can be seen in Table XI (Comtech AeroAstro, Inc.). As can be seen, this sensor is extremely small and will not add much to the mass or power requirements of the entire subsystem.

Figure 6 AeroAstro Coarse Sun Sensor[4]

Table XI AeroAstro Coarse Sun Sensor Specification

Parameter	Value
Mass (g)	10
Required Power (W)	0
Dimensions (cm)	Ø 2.286 x 0.899

[4] Image Credit: http://www.aeroastro.com/index.php/space-products-2/sun-sensors-coarse

B. Budgets

To summarize the hardware selected below are presented the mass budget and power budget of the ADCS. This system excludes reaction wheel mass and power requirements, since reaction wheels have not yet been chosen. Whoever performs the study of what reaction wheel should be chosen for the Prox-1 mission should do so with a thought to minimizing both mass and power. The Mass Budget and Power Budget are combined in Table XII.

Table XII ADCS Mass and Power Budget

Index	System	Manufacturer	Quantity	Mass per Unit (kg)	Mass Subtotal (kg)	Power per Unit (W)	Power Subtotal (W)
1	*ADCS*	--	--	--	4.442	--	10.85
1.1	*Attitude Determination System*	--	--	--	1.11	--	5.85
1.1.1	*Star Tracker*	Valley Forge	1	1	1	5	5
1.1.2	*Sun Sensor*	AeroAstro	1	0.010	0.010	0	0
1.1.3	*Magnetometer*	SpaceQuest	1	0.100	0.100	0.85	0.85
1.2	*Attitude Control System*	--	--	--	1.5	--	3
1.2.1	*Reaction Wheels*	Unknown	3	Unknown	Unknown	Unknown	Unknown
1.2.2	*Magnetic Torquers*	In-House	3	0.500	1.5	1	3
1.3	*Orbit Determination System*	--	--	--	.282	--	2
1.3.1	*GPS*	SpaceQuest	1	.200	.200	1	1
1.3.2	*GPS Antenna*	SpaceQuest	1	0.082	0.082	1	1
	Contingency				10%		10%
	Total				**2.686 kg**		**11.94 W**

C. Integration and Test

1. Functional Tests

Magnetometer

The magnetometer needs to be tested in each of its three axes. To ensure accuracy of the readings a hand held magnetometer is required. The tester should also be aware of the surroundings which could lead to magnetic anomalies. The other required equipment includes a power supply unit and data transmission cable. The procedure for this test can be seen in Table XIII.

Table XIII Magnetometer Functional Test Procedure

Step	Procedure
1	Adjust the power supply voltage to input voltage between + 20 to + 34 VDC.
2	Adjust the current limit on the power supply to allow for an input current of 50 mA.
3	Connect the X, Y and Z outputs of the magnetometer to a measuring device that has an input impedance of at least 470 KΩ. (The impedance of the magnetometer outputs is 332 Ω.)
4	Power up the magnetometer
5	Verify that the current consumption does not exceed 50 mA.
6	Orient the magnetometer such that the connector is pointing up. In this orientation, the Y arrow marked at the opposite end of the magnetometer with respect to the connector, will be pointing down. Measure the Y output of the magnetometer. The output must be roughly equal to reading from the hand held magnetometer.
7	Orient the magnetometer such that the X arrow is pointing down. Measure the X output of the magnetometer. The output must be roughly equal to reading from the hand held magnetometer.
8	Orient the magnetometer such that the Z arrow is pointing down. Measure the Z output of the magnetometer. The output must be roughly equal to reading from the hand held magnetometer.
9	Power down magnetometer.
10	Turn off power supply.
11	Return magnetometer to housing location.

Magnetic Torque Rods

The magnetic torque rods need to be tested to guarantee field uniformity and polarity. To ensure accuracy of field a hand held magnetometer is required. The tester should also be aware effects of the Earth's field on the readings. The other required equipment includes a power supply. The procedure for the functional test can be seen in Table XIV.

Table XIV Magnetic Torque Rod Functional Test

Step	Procedure
1	Take the magnetic torque rod, the power supply, and the magnetometer/computer to an open field, far away from metallic objects.
2	Set power settings on power supply. Also set current settings.
3	Power up magnetic torque rods.
4	Ensure that there are NO metal objects within 5 meters of the magnetic torque rod. Exceptions may be the power source and computer/magnetometer. Preferably, these two exceptions should be further than 1.5 meters away.
5	Hook up the magnetometer and the magnetic torque rod to a non-metallic table as shown in figure 3 of "On Determining Dipole Moments of a Magnetic Torquer Rod—Experiments and Discussions." This corresponds to R=60 cm and θ=0°.
6	Gradually increase the voltage from zero to 27 volts. Allow the reading to stabilize at each 1 volt, and record the reading (this will be the magnetic flux density).
7	After 27 volts, gradually decrease the voltage from 27 to zero volts. Allow the reading to stabilize at each 1 volt, and record the reading (this will be the magnetic flux density).
8	Wait several minutes to allow the core to desaturate (wait until the reading mirrors the reading at the beginning of the test).
9	Repeat steps 6 and 7, but this time going from 0 to -27 volts, and back up.
10	Turn off the power supply, and wait 10 minutes.

Step	Procedure
11	Repeat steps 6-9 for a second test run.
12	Repeat the whole test (steps 5-11) but this time with R=30 cm.
13	Use the formula to calculate the resulting dipole moment of the torque rod for all the data recorded.
14	Turn off power supply.
15	Disconnect everything.
16	Return magnetic torque rod to housing location.

Reaction Wheels

The reaction wheels need to be tested in a vacuum chamber. This environment will ensure they will work properly in space and to assure the drag torque. Any zero torque offset affects will then be found so as to remove these effects. This procedure can be seen in Table XV.

Table XV Reaction Wheel Functional Test Procedure

Step	Procedure
1	Place reaction wheels in vacuum chamber
2	Power up reaction wheels
3	Spin reaction wheels in a clockwise rotation to high rpms
4	Send a zero torque input.
5	Monitor reaction wheels while speeds decay to zero.
6	Repeat steps 3 thru 5 with a counterclockwise rotation
7	Power down reaction wheels
8	Return reactions wheels to housing location

Star Tracker

The star tracker needs to be tested to ensure an appropriate quaternion output. This test will be completed with the Star-Sky simulator provided by Valley Forge. More so, the test environment needs to be ESD safe and in a clean room. The other required equipment includes personal computer, power supply unit, data transmission cable, power cables for star tracker and Star-Sky simulator, and grounding wire for the Star Tracker. The procedure for the functional procedure can be seen in Table XVI.

Table XVI Star Tracker Functional Test Procedure

Step	Procedure
1	Connect the Star Tracker to the personal computer in accordance with the Star Tracker manual.
2	Connect the Star Tracker to the Star-Sky simulator in accordance with the Star Tracker manual.
3	Connect the Star Tracker to the power supply in accordance with the Star Tracker manual.
4	Connect the Star-Sky Simulator to the power supply in accordance with the Star Tracker manual.
5	Turn the computer on.
6	Turn the power supply on.
7	Establish a voltage of 27 ± 0.5 V from the power supply.
8	Start the demonstration program on the computer.

Step	Procedure
9	Turn on the star tracker via the demonstration computer in accordance with the Star Tracker manual
10	Note down the quaternion, the right ascension angle, the declination angle, and the roll angle.
11	Turn off the Star Tracker.
12	Turn off the power supply.
13	Disconnect the Star-Sky Simulator from the Star Tracker.
14	Rotate the Star-Sky Simulator 180 degrees.
15	Reconnect the Star-Sky Simulator to the Star Tracker in accordance with the Star Tracker manual.
16	Repeat steps 6 – 12.
17	Compare the two noted down values from the different runs in order to make sure that the Star Tracker responded properly to the 180 degree roll.
18	Turn off the computer.
19	Disconnect the Star-Sky Simulator from the power supply in accordance with the Star Tracker manual.
20	Disconnect the Star Tracker from the power supply in accordance with the Star Tracker manual.
21	Disconnect the Star Tracker and the Star-Sky simulator in accordance with the Star Tracker manual.
22	COVER the Star Tracker's lens with the Star Tracker lens cover.
23	Disconnect the Star Tracker from the personal computer in accordance with the Star Tracker manual.
24	Safely and securely place the star tracker back in its carrying case.

2. Integrated Tests

Coarse ADCS Integrated Test

For the coarse ADCS integrated test, a dynamic, a six degree of freedom model will be used. Simulated outputs for the magnetometer will be used and will input into the developed algorithms for coarse attitude determination. The determine coarse attitude will then input into the coarse attitude control algorithms which will instruct the simulated satellite to move according to the magnetic field that would be created by the torque rods. The torque rods can also be directly connected to the coarse attitude control algorithms to make sure that they create the magnetic moment predicated.

Fine ADCS Integrated Test

For the fine ADCS integrated test, a six degree of freedom model will be used. Simulated outputs for the star tracker will be used and will input into the developed algorithms for fine attitude determination. The determined fine attitude will then input into the fine attitude control algorithms which will instruct the simulated satellite to move according to the angular momentum that would be created by the reaction wheels.

V. Algorithms

An attitude determination and control system is not defined by hardware alone. As discussed in the ADCS architecture section of this paper, different pieces of hardware dictate that different algorithms must be used. A Kalman Filter must be used to get full attitude knowledge from a magnetometer; a control law must be developed to change the attitude, etc. In this section of the paper, these algorithms will be defined and discussed.

A. Definition of Reference Frames

In this section the reference frames used in the algorithms and throughout this paper are defined. It should be noted that coordinate transformations are not detailed in this section. Coordinate transformations are explained in the appropriate algorithms, so that the entire algorithm is explained in one section rather than pieced out. Also, coordinate transformations between every coordinate frame listed are unnecessary. So coordinate transformations will only be explained as they become necessary.

1. EME J2000

An inertial reference frame is often needed for calculations, since an inertial reference frame is a frame that is non-accelerating. For the sake of the work in this paper, an Earth-Centered Inertial frame is used. This is a reference frame that is centered at the Earth but does not rotate with the Earth (Bate, Mueller, & White, 1971). Though in a grander sense, this frame does rotate, since the Earth rotates about the sun and even our solar system rotates about the center of our galaxy, it is generally accepted that in Earth-orbiting spacecraft, this reference frame can be used as an inertial reference frame (Bate, Mueller, & White, 1971).

To define a reference frame, more than a center, like the Earth, needs to be defined. The x-y plane needs to be defined as well as the x-axis and z-axis; the y-axis is then defined according to the right hand rule. The x-y plane for this frame is the Earth mean equator (Bate, Mueller, & White, 1971). The x-direction is defined as the Equinox of January 1, 2000 at noon (Bate, Mueller, & White, 1971). The z-axis is aligned with the Earth's spin axis in the direction of the North Pole (Bate, Mueller, & White, 1971). This reference frame will herein be described as EME J2000 (short for Earth mean equator January 2000) and can be seen visually in Figure 7.

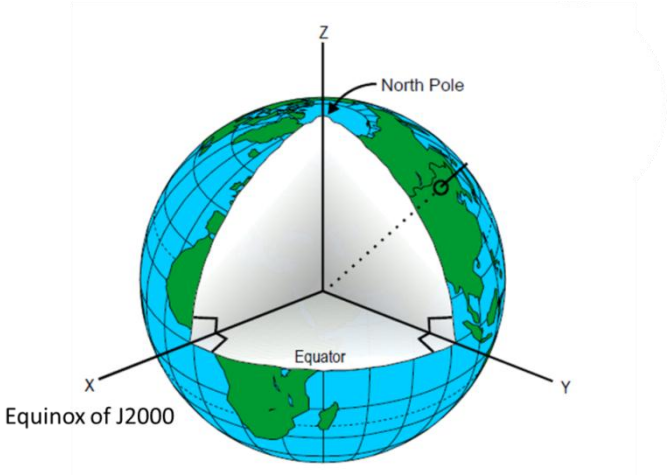

Figure 7 EME J2000 Coordinate Frame[5]

2. ECEF

It is often convenient to define an Earth centered frame that rotates with the Earth, rather than being inertial like the EMI J2000 frame. This frame is very similar to the EMI J2000 frame, except it rotates with the Earth. The x-y plane is still defined as the Earth-mean equator, and the z-axis is aligned with the North Pole (Bate, Mueller, & White, 1971). The x-axis crosses through the point where the Prime Meridian and the Earth's equator meet (Bate, Mueller, & White, 1971). And the y-axis is defined according to the right-hand rule, as can be seen in Figure 8. This frame will herein be called ECEF, i.e. Earth-Centered, Earth-Fixed.

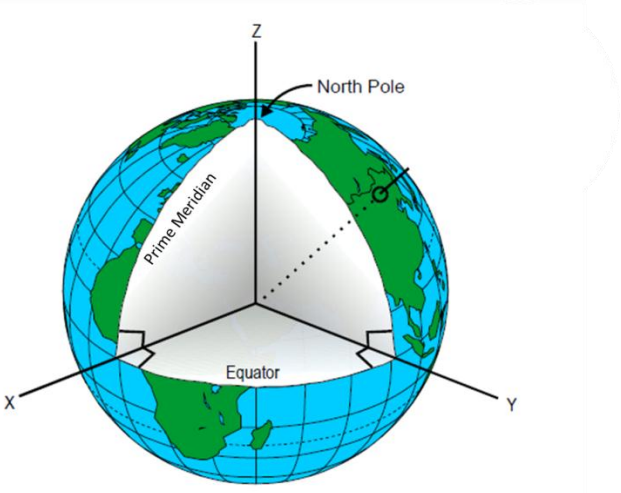

Figure 8 ECEF Coordinate Frame[6]

[5] Image Credit: http://en.wikipedia.org/wiki/Earth-centered_inertial (Equinox Label was added by the author of this paper)

3. Geodetic Frame

The geodetic frame where coordinates are described in latitude, longitude, and height is not often convenient for satellites, but sometimes it is necessary. The magnetic field model used in the algorithms requires the position to be input in this coordinate frame; therefore, this frame is necessary. This is a spherical coordinate system, so it is defined differently from the others. To describe the position two angles, the latitude and longitude, and the height are needed. Latitude is defined as positive above the equator and negative below the equator. Longitude is described as positive when going east from the Prime Meridian and negative when going west. Height is the altitude above the Earth's surface. This frame can be seen visually in Figure 9.

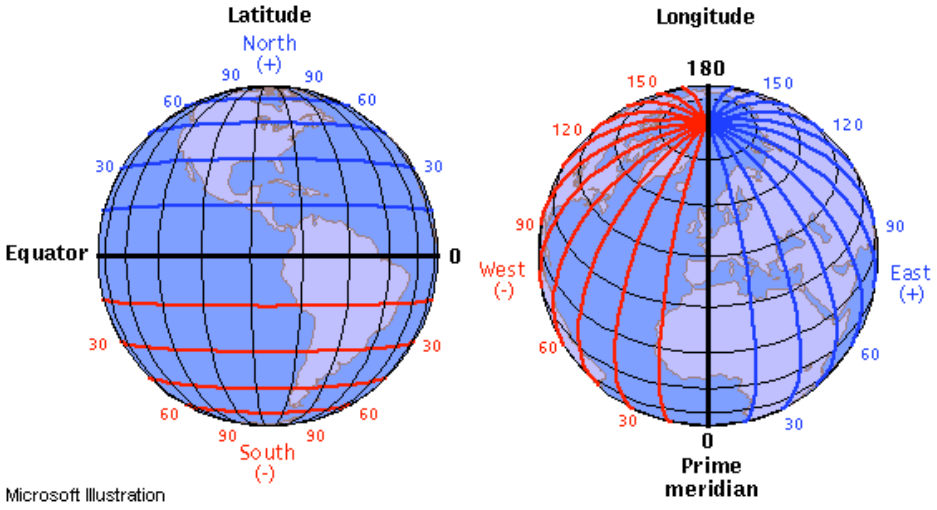

Figure 9 Geodetic Coordinate Frame[7]

4. LVLH Frame

The local-vertical, local-horizontal frame, henceforth known as LVLH frame, is a spacecraft centered frame. It is defined by the idea of a local vertical, i.e. a line that connects the spacecraft's center to the center of the body it's orbiting. The z-axis is defined on this local vertical as a line from the spacecraft to the body, which is for the most part the nadir direction. The x-direction is along the local horizontal, which is a line that is tangent to the orbit. The x-direction is defined in the direction of the orbit. The y-axis is then defined according to the right hand rule. This can be seen visually in Figure 10.

---

[6] Image Credit: http://en.wikipedia.org/wiki/Earth-centered_inertial (Prime Meridian Label was added by the author of this paper)

[7] Image Credit: http://www.learner.org/jnorth/tm/LongitudeIntro.html

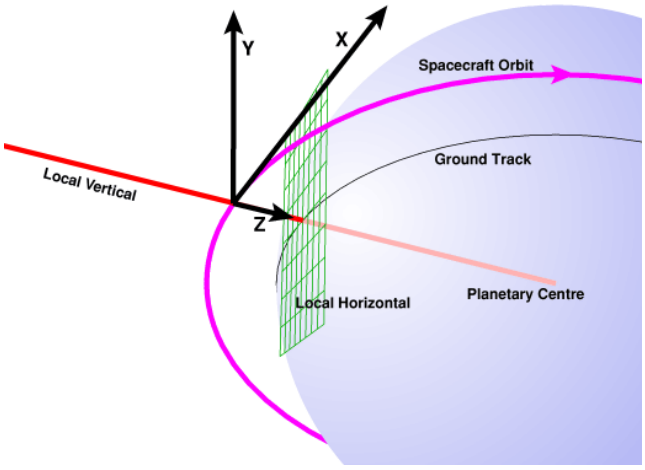

Figure 10 LVLH Coordinate Frame[8]

5. NED Frame

A north-east-down frame, or NED for short, is not often the most convenient frame. However, it is the frame in which the World Magnetic Model outputs the magnetic field vector. It is important to note that this is a spacecraft centered frame, but it's a spacecraft centered frame with its coordinates defined differently from the previously mentioned spacecraft centered frame (Maus, et al., 2010). One aspect between the two frames is similar. The z-axis points in the zenith direction, or down as it's called in the coordinate frame name (Maus, et al., 2010). The x-axis points towards true north, i.e. the geographic north, and then the y-axis points in the easterly direction, as dictated by the right hand rule (Maus, et al., 2010).

6. Body Fixed Frame

The body fixed frame is a frame that is centered on the spacecraft body and fixed to it. It is centered at the spacecraft's center of gravity and the z-axis is defined as pointing down through the spacecraft's nadir face. The choice for the x-axis and y-axis direction are somewhat arbitrary, as long as they following the right hand rule. Since at the time this paper is being written, the structure has not yet been finalized, it is hard to define these two. The x-axis should be defined as pointing through the center of an arbitrary side plate, and the y-axis is defined according to the right hand rule. The arbitrary side plate can be selected once the structure is finalized. For the algorithms to be defined, it truly is arbitrary, and therefore, the side can be selected at a later date. It should be noted that when roll, pitch, and yaw are zero, this frame aligns with the LVLH frame.

[8] Image Credit: http://www.ehartwell.com/afj/LVLH_%28Local_Vertical/Local_Horizontal%29

B. Coarse ADCS

1. Coarse ADCS Detumble Analysis

To determine the length of time it will take the spacecraft to detumble an analysis must be done. However, because the structural design of the Prox-1 spacecraft is, at the time of this report, not complete, and to this author's knowledge an orbital analysis has not be done, the analysis presented here will be the analysis done for the R^3 mission. The author feels this is important to include so that the method of the analysis is not lost and can be reapplied to Prox-1 once designs are finalized.

A rough analysis was performed in order to determine an estimate of how long it will take the R^3 spacecraft to detumble. Eventually it is hopes that a time domain simulation will be created to simulate detumble; however, for this analysis a conservative, back-of-the-envelope calculation was done.

For Low Earth Orbit (LEO), the field strength of the Earth is between 250 mG and 500 mG. The lower number was assumed since this is the more conservative number. Lower magnetic fields mean that less momentum will be dumped. Equation 3 was used to calculate the magnitude of the torque created by the torque rods using this magnetic field value, where m is the dipole moment and B is the magnetic field. Using the dipole moment of 10 Am^2 and the low magnetic field, a torque of 0.25 mN-m was found.

$$T = m \times B \tag{1}$$

An orbit length of 90 to 97 minutes was determined by the mission design team. From orbit length, the amount of momentum that can be dumped per orbit can be determined using equation 4. From this it was determined that for a 90 minute orbit 0.9 N-m-s could be dumped, and for a 97 minute orbit 0.97 N-m-s could be dumped. It should be noted that the two-third term in the equation is to take into account that a satellite cannot always dump momentum. This term assumed that momentum can be dumped during two-thirds of the orbit.

$$Momentum\ dumped\ per\ orbit = 2/3(T * Orbit\ length\ (in\ seconds)) \tag{2}$$

Now in order to figure out how long it takes the satellite to dump this momentum, the amount of momentum that the satellite will have needs to be determined. To find the angular momentum of the satellite Equation 3 was used, where L is the angular momentum, I is the moment of inertia, and w is the angular velocity in radians per second. The moment of inertias were provided by the structures team and can be seen in Table XVII.

$$L = I \times \omega \tag{3}$$

Table XVII Moment of Inertia Values for the R^3 satellite

Moment of Inertia	Value (kgm^2)
I_{xx}	3.78
I_{yy}	3.80
I_{zz}	1.21

The highest moment of inertia is the worst case moment, therefore 3.80 was rounded to 4 in order to be more conservative. Now the angular velocity must be found. A survey of launch vehicles was done and it seems that the highest (worst case) angular velocity possible is five degree per second. Assuming this worst case angular rate happens completely about our worst case moment of inertia axis, an angular momentum of 0.349 N-m-s was found. Dividing this number by the momentum that could be dumped per orbit gives the percent of the orbit it will take to dump the momentum. These numbers turn out to be 39% and 37% of one orbit for the 90 minute and 97 minute orbits, respectively. A generous safety factor of 5 was placed on these numbers, bringing these numbers to 1.8 and 1.9 orbits. Therefore, it is found that it will take approximately 3 hours to detumble, whether at a 90 minute orbit or a 97 minute orbit.

2. Control Law Development

Equations of Motion

When creating an attitude determination and control system, the first step is to define the equations of motion for the system in question. The Prox-1 satellite is a rigid-body. The dynamics of a rigid-body satellite are described by Equation 4.

$$\vec{M} = \hat{J} \cdot \dot{\vec{\omega}} + \vec{\omega} \times \hat{J} \cdot \vec{\omega} \tag{4}$$

where J is the moment of inertia matrix and ω is the angular velocity of the spacecraft, where the angular velocity is the angular velocity of the body fixed frame with respect to the ECEF, also notated as $\omega^{B/N}$ (Wie, 1998). During coarse control modes, we can assume a circular orbit around the earth. Because of this we must add a gravity gradient torque term, as seen in Equation 5 (Wie, 1998).

$$\vec{M} = 3n^2 \vec{a}_3 \times \hat{J}\vec{a}_3 \tag{5}$$

Combining these two equations, i.e. setting them equal to each other gives the full equations of motion for the Prox-1 spacecraft. However, they present a problem in that they are non-linear. Non-linear dynamics are highly complicated and difficult to work with when creating a control law. It is common practice to linearize non-linear

equations so that they fit into the state-space format of equations, which can be seen in Equation 6. Linearizing the equations into this format is not a bad assumption, since over short periods, the system can be viewed as linear. Controls is a fast paced system dealing in small periods of time.

$$\dot{x} = Ax + Bu \tag{6}$$

Thus, the equations of motion are linearized and, when broken up per axis, yield the following equations (Wie, 1998):

$$J_1\ddot{\emptyset} + a\emptyset + b\dot{\psi} = u_1 + T_{d_1} \tag{7}$$

$$J_2\ddot{\theta} + d\theta = u_2 + T_{d_2} \tag{8}$$

$$J_3\ddot{\psi} + c\psi + b\dot{\emptyset} = u_3 + T_{d_3} \tag{9}$$

J_1, J_2, and J_3 are the components of J. T_{d1}, T_{d2}, and T_{d3} are the disturbance torques about each access, and u_1, u_2, and u_3 are the calculated control torques (Wie, 1998). θ, Φ, and ψ are the three Euler angles, also known as pitch, roll, and yaw angles, respectively (Wie, 1998). These angles are with respect to the Spacecraft Fixed Frame (Wie, 1998). The remaining constants, a, b, c, and d, are defined below (Wie, 1998).

$$a = 4n^2(J_2 - J_3) \tag{10}$$

$$b = -n(J_1 - J_2 + J_3) \tag{11}$$

$$c = n^2(J_2 - J_1) \tag{12}$$

$$d = 3n^2(J_1 - J_3) \tag{13}$$

$$n = \sqrt{\frac{\mu}{(R_e+h)^3}} \tag{14}$$

Where Re is the radius of the Earth, h is the altitude of the spacecraft, and μ is the Earth's gravitation parameter, i.e. 398,600 km^3/s^2 (Bate, Mueller, & White, 1971). The full derivation of the linearized equations of motion can be found in *Space Vehicle Dynamics and Control* by Bong Wie.

Now we have the set of equations that describe the movement of our system. These are the equations used to propagate forward the system, to determine and predict the attitude. However, determination and predication are the not the goals of this system. The goal is control. In order to control the system, the control torques, which will be input into Equations 7 through 9, must be determined.

Theoretical Control Torque Calculation

Though exotic and complex control laws do exist for a system of torque rods, most of these exotic and complex control laws are untested in space. Some control laws are also specific to spin stabilization, such as a B-dot control law, and other control laws are developed for one specific sort of pointing, like sun pointing. Therefore, a PD controller was selected as the best fit for this system.

A PD controller is defined as a controller that has a proportional gain and a gain on the derivative, such as in Equation 15, where x is the variable being controlled, k_p is the proportional gain, and k_d is the derivative gain.

$$u = -k_p x - k_d \dot{x} \tag{15}$$

When calculating the gains, two rules were developed. First, the steady-state error of the attitude angles due to constant disturbance torques must be limited to a maximum value, and second, the closed-loop damping ration must be equal to the ideal value of $\sqrt{2}/2$.

It is important to note here that attitude is being described via Euler angles. The Euler angles describe the orientation of the body-fixed reference frame with respect to the LVLH frame. The rotational sequence 3-2-1 is used to get to the body-fixed reference frame from the LVLH reference frame.

When determining the control torques, it is logical to start with the pitch attitude angle, since it is not coupled with the other angles, as can be seen in Equation 8. The control torque for the pitch is therefore:

$$u_2 = -k_{p2}\theta - k_{d2}\dot{\theta} \tag{16}$$

To derive the gains, Equation 16 must be substituted into Equation 8 and then the Laplace Transform taken to find the transfer function. It is worthy to note that this assumes null initial conditions, as is always true in a transfer function. The result is Equation 17, where ξ is the damping ration and ω_n is the natural frequency of the closed-loop system (Nise, 2004).

$$\frac{\theta(s)}{T_{d_2}(s)} = \frac{1/J_2}{s^2 + \frac{k_{d2}}{J_2}s + \frac{k_{p2}+d}{J_2}} = \frac{1/J_2}{s^2 + 2\xi\omega_n s + \omega_n^2} \tag{17}$$

Next, the steady-state error of the pitch attitude angle is calculated, using the final-value theorem, as can be seen in Equation 18 where T_{d20} is the constant value of the disturbance torque and θ_{ss} is the maximum value of the steady-state error for the pitch attitude angle.

$$\lim_{t\to\infty} \theta(t) = \lim_{s\to 0} s\theta(s) = \lim_{s\to 0} s \frac{\theta(s)}{T_{d_2}(s)} \frac{T_{d_2}}{s} = \frac{T_{d_{20}}}{k_{p2}+d} = \theta_{ss} \tag{18}$$

This equation can then be rearranged to yield our proportional gain, as can be seen in Equation 16. It is worth reminding at this point that d is the constant calculated in Equation 19.

$$k_{p2} = \frac{T_{d_{20}}}{\theta_{ss}} - d \tag{19}$$

In order to get the derivative gain, the relations established in Equation 17 can be used, which yields Equation 20.

$$k_{2d} = 2\xi J_2 \sqrt{\frac{k_{2p}+d}{J_2}} \tag{20}$$

Thus, the control torque for the pitch angle can be calculated. Now it is time to move onto the roll and yaw angles, which as was stated before, are coupled. The control torques are given by the following expressions:

$$u_1 = -k_{p1}\emptyset - k_{d1}\dot{\emptyset} \tag{21}$$

$$u_3 = -k_{p3}\psi - k_{d3}\dot{\psi} \tag{22}$$

Plugging Equations 21 and 22 into Equations 7 and 9, respectively, and then performing a Laplace Transform, yields the following equations:

$$\emptyset(s) = \frac{\frac{1}{J_1}s^2 + \frac{k_{d3}}{J_1 J_3}s + \frac{c+k_{p3}}{J_1 J_3}}{\Delta(s)} T_{d_1}(s) + \frac{-\frac{b}{J_1 J_3}s}{\Delta(s)} T_{d_3}(s) \tag{23}$$

$$\psi(s) = \frac{\frac{b}{J_1 J_3}s}{\Delta(s)} T_{d_1}(s) + \frac{\frac{1}{J_3}s^2 + \frac{k_{d1}}{J_1 J_3}s + \frac{a+k_{p1}}{J_1 J_3}}{\Delta(s)} T_{d_3}(s) \tag{24}$$

$$\Delta(s) = s^4 + \left(\frac{k_{d1}J_3 + J_1 k_{d3}}{J_1 J_3}\right)s^3 + \left(\frac{J_1 c + J_1 k_{p3} + aJ_3 + k_{p1}J_3 + k_{d1}k_{d3} + b^2}{J_1 J_3}\right)s^2 +$$

$$\left(\frac{k_{p1}k_{d3} + k_{d1}c + k_{d1}k_{p3} + ak_{d3}}{J_1 J_3}\right)s + \left(\frac{k_{p1}c + k_{p1}k_{p3} + ac + ak_{p3}}{J_1 J_3}\right) \tag{25}$$

The final-value theorem can be applied to Equations 23 and 24 to find the steady-state errors of the roll and yaw angles, as can be seen in Equations 26 and 27.

$$\lim_{t\to\infty} \emptyset(t) = \lim_{s\to 0} s\emptyset(s) = \frac{c+k_{p3}}{k_{p1}c + k_{p1}k_{p3} + ac + ak_{p3}} T_{d_{10}} = \emptyset_{ss} \tag{26}$$

$$\lim_{t\to\infty} \psi(t) = \lim_{s\to 0} s\psi(s) = \frac{c+k_{p1}}{k_{p1}c + k_{p1}k_{p3} + ac + ak_{p3}} T_{d_{30}} = \psi_{ss} \tag{27}$$

As in the previous equations, T_{d10} and T_{d30} are the constant disturbance torques, and Φ_{ss} and ψ_{ss} are the maximum values of the steady-state errors. Equations 26 and 27 can then be rearranged to find the proportional gains, which can be seen in Equations 28 and 29.

$$k_{p1} = \frac{1-\frac{\emptyset_{ss}}{T_{d_{10}}}a}{\emptyset_{ss}/T_{d_{10}}} \tag{28}$$

$$k_{p3} = \frac{1-\frac{\psi_{ss}}{T_{d_{30}}}c}{\psi_{ss}/T_{d_{30}}} \tag{29}$$

To find the derivative gains, Equation 25 is rearranged into canonical form, which can be seen in Equation 30 (Nise, 2004).

$$\Delta(s) = s^4 + 2\left(\xi_1\omega_{n_1} + \xi_2\omega_{n_2}\right)s^3 + \left(\omega_{n_1}^2 + \omega_{n_2}^2 + 4\xi_1\xi_2\omega_{n_1}\omega_{n_2}\right)s^2 + 2\omega_{n_1}\omega_{n_2}\left(\xi_1\omega_{n_1} + \xi_2\omega_{n_1}\right)s + \omega_{n_1}^2\omega_{n_2}^2 \tag{30}$$

If $\xi_1=\xi_2=\xi=\sqrt{2}/2$ is imposed, then it becomes a system of four equations and four unknowns that can be solved to find the derivative gains. If the system is solved, the derivative gains are found, as can be seen in Equations 31 and 32.

$$k_{d1} = \sqrt{\frac{8uJ_1^2J_3^2\xi^2+4v\xi^2J_1J_3-16\xi^4uJ_1^2J_3^2}{J_3^2+J_1^2w^2+2J_3J_1w-4w\xi^2J_1J_3}} \tag{31}$$

$$k_{d3} = wk_{d1} \tag{32}$$

where u, v, and w are defined by Equations 33, 34, and 35, respectively.

$$u = \sqrt{\frac{1}{J_1J_2}\left(k_{p1}c + k_{p1}k_{p3} + ac + ak_{p3}\right)} \tag{33}$$

$$v = J_1c + J_1k_{p3} + aJ_3 + k_{p1}J_3 + b^2 \tag{34}$$

$$w = \frac{-uJ_3+c+k_{p3}}{uJ_1-k_{p1}-a} \tag{35}$$

With these gains, the theoretical, perfect control torque to input into the state space equation has been found. However, the system is not a theoretical, perfect system. It is system composed of torque rods.

Real Torque Calculation

Finding the theoretical torque is a necessary first step to finding the actual torque needed. In order to get from the theoretical torque to real torque, how torque rods create torque must be recalled, which is according to

Equation 36, where m is the magnetic moment of the torque rod and b is the strength of the Earth's magnetic field (Wertz, Spacecraft Attitude Determination and Control, 1978).

$$u = m \times b \tag{36}$$

The magnetic moment of the torque rod is known, as part of the torque rod specification. However, to find the strength of the Earth's magnetic field, a model for the Earth's magnetic field must be used. The model used in this analysis is the World Magnetic Model, which is available in Matlab.

In order to know the vector for the Earth's magnetic field at any point, it is necessary to know not just the spacecraft's attitude but its position in orbit around the Earth, since the magnetic field is dependent upon the position. Therefore, in the algorithm, the earth's orbit must be propagated. For the purpose of this algorithm, a basic orbit propagation was developed. Since the time interval over which the propagation takes place is small, it was determined that third body and Earth oblateness terms did not need to be considered.

The propagator takes in the initial orbital elements, the gravitational parameter, and the time in the future that the orbit needs to be propagated to. The orbital elements are a, e, *i*, Ω, ω, and ν, which are the semi-major axis, the eccentricity, the inclination, the longitude of the ascending node, the argument of periapse, and the true anomaly, respectively. The orbital elements are converted into a position and velocity in the EME J2000 frame using the following equations, where r and v are the position and velocity in the EME J2000 frame, respectively (Bate, Mueller, & White, 1971):

$$r = \begin{bmatrix} \cos\Omega & \sin\Omega & 0 \\ -\sin\Omega & \cos\Omega & 0 \\ 0 & 0 & 1 \end{bmatrix} \begin{bmatrix} 1 & 0 & 0 \\ 0 & \cos i & -\sin i \\ 0 & \sin i & \cos i \end{bmatrix} \begin{bmatrix} \cos\omega & \sin\omega & 0 \\ -\sin\omega & \cos\omega & 0 \\ 0 & 0 & 1 \end{bmatrix} \begin{bmatrix} \frac{a(1-e^2)}{1+e\cos\nu}\cos\nu \\ \frac{a(1-e^2)}{1+e\cos\nu}\sin\nu \\ 0 \end{bmatrix} \tag{37}$$

$$v = \begin{bmatrix} \cos\Omega & \sin\Omega & 0 \\ -\sin\Omega & \cos\Omega & 0 \\ 0 & 0 & 1 \end{bmatrix} \begin{bmatrix} 1 & 0 & 0 \\ 0 & \cos i & -\sin i \\ 0 & \sin i & \cos i \end{bmatrix} \begin{bmatrix} \cos\omega & \sin\omega & 0 \\ -\sin\omega & \cos\omega & 0 \\ 0 & 0 & 1 \end{bmatrix} \begin{bmatrix} \sqrt{\frac{\mu}{a(1-e^2)}}\sin\nu \\ \sqrt{\frac{\mu}{a(1-e^2)}}(1+e\cos\nu) \\ 0 \end{bmatrix} \tag{38}$$

With the position and velocity known as well as the time in the future to which the position and velocity must be propagated and can be using the following equations for the derivatives of position and velocity (Bate, Mueller, & White, 1971):

$$\dot{r} = v \tag{39}$$

$$\dot{v} = \frac{-\mu}{\|r\|} r \tag{40}$$

With these equations, the propagated orbit at the specified time is found in the EME J2000 frame.

Unfortunately, the World Magnetic Model requires an input in the geodetic coordinate frame, previously described in this paper. Therefore, the position must be transformed from the EME J2000 frame to the geodetic frame. It is worthy to note that the World Magnetic Model does not need the velocity of the spacecraft, only the position. Therefore, in the algorithm, velocity will be discarded and only position will be transformed into the appropriate coordinate frame.

Transforming from the EME J2000 frame to the geodetic frame is not trivial; therefore, it will be approached in two steps. First, the position shall be transformed from the EME J2000 frame to the ECEF frame. Then the position will be transformed from the ECEF frame to the geodetic frame.

To transform from EME J2000 and ECEF frame, the first step is to transform the date from the regular format of a date, i.e. Month Day, Year, to a Julian Date. A Julian Date is a measurement of time used by astronomers, which is a continuous count of days from January 1, 4713 BC (Wertz, Spacecraft Attitude Determination and Control, 1978). The use of Julian Date is so common, that Matlab actually has a built in function for it, which is the function used in the algorithm. It is also worthy to note that a date had to be assumed in the algorithm to make them function properly; therefore, for ease the date was selected to October 31, 2011 and the start time was chosen to be 0:00.

Once the Julian Date is calculated, a value, T, is created, which is essentially the amount of time that has transpired since January 1, 2000. This is the time the EME J2000 frame is based upon. The calculation is done using the following equation (Vallado, 2007):

$$T = \frac{JulianDate - 2451535}{36525} \tag{41}$$

Another important delta time must also be calculated, which is the amount of time that has passed since the zero hour of the day, i.e. midnight. It is important that this time be in seconds, as in the total number of seconds to pass since midnight of that day. The importance of the unit is for its use in later equations. The next step is to calculate the sidereal time at the zero hour of the day, using the following equation (Vallado, 2007):

$$\theta_{g_0} = 24110.54841 + 8640184.812866T + 0.093104T^2 - (6.2 \cdot 10^{-6})T^3 \tag{42}$$

Then this zero hour sidereal time needs to be converted to the sidereal time at our current time, using Equation 43 (Vallado, 2007). It is important to note that this sidereal time, is an angle which is in radians.

$$\theta = \theta_{g_0} + (7.29211510 \cdot 10^{-5})\Delta t \tag{43}$$

With the sidereal time the orbit can be transformed, using Equation 44 (Vallado, 2007).

$$R_{ECEF} = \begin{bmatrix} \cos\theta & \sin\theta & 0 \\ -\sin\theta & \cos\theta & 0 \\ 0 & 0 & 1 \end{bmatrix} R_{EMEJ2000} \tag{44}$$

Thus the position has been transformed from the EME J2000 coordinate frame to the ECEF.

However, another transformation must still be performed: the transformation from the ECEF to the geodetic frame. Fortunately, Simulink has a built in function that does this. It takes in the ECEF position and outputs the geodetic latitude and longitude as well as the orbit altitude. Explanation of the algorithm used can be found in the documentation on the MathWorks website.

Thus now the orbital position is in a coordinate system that can be used by the World Magnetic Model. The world magnetic model takes in this position as well as the decimal year, which is the desired year in decimal format that includes any fraction of the year that has already passed. The model can then calculate a variety of outputs, but for the sake of this algorithm, the only output cared about is the magnetic field vector in nanotesla. However, having just spent some time with coordinate transformations, it must be ensured that this magnetic field vector is in the correct coordinate frame to be used in our model.

Remember, from the earlier discussion of Euler Angles, that the theoretical control torques are calculated using Euler Angles based in the LVLH frame. This is a different reference frame from the NED frame, though at certain orbits and certain points the two frames can be identical. Therefore, an orbit transformation between the NED frame to the LVLH frame must be created to get the magnetic field in the same frame as the control torques.

Unfortunately, this is not a one-step transformation. To get from the NED frame to the LVLH frame, first the vector must be transformed to the ECEF frame, using the following transformation:

$$v_{ECEF} = R^{-1} v_{NED} \tag{45}$$

where v_{ecef} is the vector in the ECEF frame and v_{NED} is the vector in the NED frame. R is the matrix defined by the following equation, where *lat* is the latitude and *lon* is the longitude:

$$R = \begin{bmatrix} \cos(-90) & 0 & -\sin(-90) \\ 0 & 1 & 0 \\ \sin(-90) & 0 & \cos(-90) \end{bmatrix} \begin{bmatrix} \cos(-lat) & 0 & -\sin(-lat) \\ 0 & 1 & 0 \\ \sin(-lat) & 0 & \cos(-lat) \end{bmatrix} \begin{bmatrix} \cos(lon) & \sin(lon) & 0 \\ -\sin(lon) & \cos(lon) & 0 \\ 0 & 0 & 1 \end{bmatrix} \tag{46}$$

From the ECEF frame, the vector can be transformed to the EME J2000 frame using the following transformation, where θ is the sidereal time as calculated in Equation 43:

$$v_{EME} = \begin{bmatrix} \cos(-\theta) & \sin(-\theta) & 0 \\ -\sin(-\theta) & \cos(-\theta) & 0 \\ 0 & 0 & 1 \end{bmatrix} v_{ECEF} \tag{47}$$

From the EME J2000 frame the vector can be transformed to the LVLH frame using the following transformation:

$$v_{LVLH} =$$

$$\begin{bmatrix} \cos(-90) & \sin(-90) & 0 \\ -\sin(-90) & \cos(-90) & 0 \\ 0 & 0 & 1 \end{bmatrix} * \begin{bmatrix} \cos(-90) & 0 & -\sin(-90) \\ 0 & 1 & 0 \\ \sin(-90) & 0 & \cos(-90) \end{bmatrix} * \begin{bmatrix} \cos(\nu) & \sin(\nu) & 0 \\ -\sin(\nu) & \cos(\nu) & 0 \\ 0 & 0 & 1 \end{bmatrix} *$$

$$\begin{bmatrix} \cos(\omega) & \sin(\omega) & 0 \\ -\sin(\omega) & \cos(\omega) & 0 \\ 0 & 0 & 1 \end{bmatrix} * \begin{bmatrix} 1 & 0 & 0 \\ 0 & \cos(i) & \sin(i) \\ 0 & -\sin(i) & \cos(i) \end{bmatrix} * \begin{bmatrix} \cos(\Omega) & \sin(\Omega) & 0 \\ -\sin(\Omega) & \cos(\Omega) & 0 \\ 0 & 0 & 1 \end{bmatrix} v_{EME} \tag{48}$$

Now the magnetic field is in the LVLH frame. However, the magnetic field actually needs to be in the body frame, i.e. the frame where the pitch, roll, and yaw angles are applied to transform from LVLH. This is done using the next, final transformation, remember that in this equation θ is the pitch angle:

$$v_{BodyFixed} = \begin{bmatrix} 1 & 0 & 0 \\ 0 & \cos(\Phi) & \sin(\Phi) \\ 0 & -\sin(\Phi) & \cos(\Phi) \end{bmatrix} \begin{bmatrix} \cos(\theta) & 0 & -\sin(\theta) \\ 0 & 1 & 0 \\ \sin(\theta) & 0 & \cos(\theta) \end{bmatrix} \begin{bmatrix} \cos(\psi) & \sin(\psi) & 0 \\ -\sin(\psi) & \cos(\psi) & 0 \\ 0 & 0 & 1 \end{bmatrix} v_{LVLH} \tag{49}$$

Now that the magnetic field is in the spacecraft body fixed frame, the torque limits can be calculated, i.e. the maximum and minimum torques the torque rod can produce. The calculation of the torque limits is fairly simple. Torque rods produce torque based on Equation 36. Recalling the discussion of the torque rod hardware, the magnetic moment of the torque rods is 10 Am^2. Since there is a torque rod in each direction, a 10 Am^2 magnetic moment is available in every body-fixed direction. Crossing this vector of magnetic moments with the magnetic field vector previously determined gives the maximum torque for all three directions. To get the minimum torque the polarity of the torque rods is switched, making the magnetic moment -10 Am^2, and the same cross product is performed.

The theoretical torque values are then compared to these maximum and minimum torque values. If the theoretical torque value is between the maximum and minimum value, then it is the torque that should be applied to the system. If it is outside of this bounded area, then the maximum or minimum torque, as appropriate, becomes the applied torque.

3. Kalman Filter

From the previous analysis, it is clear that the attitude cannot be corrected unless it is initially known. However, from a magnetometer reading alone, only the Euler angles and not the rates of rotation can be derived. In order to have full attitude knowledge, the Euler angles as well as the rates of rotation need to be known. Adding a sensor to find rates is a feasible solution, but a costly one that adds mass to the satellite. Since the satellite architecture determined the low cost, low mass magnetometer only determination system, a solution must be found to this problem without additional sensors.

A Kalman Filter is a recursive solution to the problem of filtering linear discrete data (Welch & Bishop, 2001). A satellite system is not linear but in the previous discussion it was linearized. Therefore, it can be treated as a linear system. Essentially, what a Kalman Filter does is predict the attitude state of the satellite and then correct that predicted state based on the input of the sensor, in this case the magnetometer (Welch & Bishop, 2001). Essentially, the Filter has two steps: "predict" and "correct".

Initially the state of the satellite is estimated and also a variable called the error covariance must be estimated. The estimated state is then used to predict the state using the following equation:

$$\hat{x}_k^- = \Phi \hat{x}_{k-1} + B u_k \Delta t \tag{50}$$

where x is the state, k denotes the time step which means k-1 is the state from the previous time step, the – symbol after x_k denotes that it is the predicted attitude also known as the attitude before correction, Δt is the time step, B is the same as in Equation 6, u_k is the commanded torque at the time, and Φ is the state transition matrix (Welch & Bishop, 2001) (Vallado, 2007). It's clear from this equation that this Filter relies on our previous calculation of the predicted torque. This does not require a complete control algorithm but rather the subset of it that predicts the control torque at a specific time step. The state transition matrix can then be estimated by the following equation, where A is the matrix from Equation 6 (Hart, 2007):

$$\Phi \approx I + A\Delta t \tag{51}$$

Now the error covariance can be calculated using the following equation:

$$P_k^- = \Phi P_{k-1} \Phi^T + Q \tag{52}$$

where P is the error covariance matrix and Q is the process noise covariance (Welch & Bishop, 2001). These two equations encompass the "predict" step. Now that the attitude and error covariance has been predicted, the attitude must be corrected based on the measurement.

The first item to be calculated during the "correct" step is the Kalman gain as seen in the following equation:

$$K_k = P_k^- {H_k}^T \left(H_k P_k^- {H_k}^T + R\right)^{-1} \tag{53}$$

where H_k is the observation matrix at the current time step and R is the measurement noise covariance (Welch & Bishop, 2001). Next the attitude state is updated with the measurement taken by the magnetometer, which is denoted by z (Welch & Bishop, 2001).

$$\hat{x}_k = \hat{x}_k^- + K_k(z_k - H_k\hat{x}_k^-) \tag{54}$$

With the Kalman Filter gain known, the error covariance can then be updated using the following equation, where I is merely the identity matrix (Welch & Bishop, 2001).

$$P_k = (I - K_k H_k)P_k^- \tag{55}$$

Now, the new state and error covariance matrix can be inputting into the "predict" step to start the process over again (Welch & Bishop, 2001).

It can be seen that most of the values are calculated or known. However, before the algorithm can be started H_k, R, and Q must be determined, and a guess for attitude state and error covariance must be made. But before those values can be calculated our state vector must be discussed.

For Kalman Filtering, it is far more common to use the quaternion representation of the attitude than the Euler Angle attitude. Recalling that a quaternion has four terms, a scalar term (q_4) and three vector terms (q_1, q_2, q_3), the state vector then becomes the following, where $\vec{\omega}$ is the attitude rate vector (Sturm II, 2005):

$$x = \begin{bmatrix} q \\ \vec{\omega} \end{bmatrix} = \begin{bmatrix} q_1 \\ q_2 \\ q_3 \\ q_4 \\ \omega_1 \\ \omega_2 \\ \omega_3 \end{bmatrix} \tag{56}$$

Various previous papers have determined that using the full representation of the state is unwieldy. However, this state vector can be reduced into a new state, $\tilde{x}$, which can be seen in the following equation (Sturm II, 2005):

$$\tilde{x} = \begin{bmatrix} \partial\vec{q} \\ \vec{\omega} \end{bmatrix} = \begin{bmatrix} \partial q_1 \\ \partial q_2 \\ \partial q_3 \\ \omega_1 \\ \omega_2 \\ \omega_3 \end{bmatrix} \tag{57}$$

where $\partial\vec{q}$ is the vector part of our reduced quaternion. The fourth term of the reduced quaternion can be found according to the following equation (Sturm II, 2005):

$$\delta q_4 = \sqrt{1 - \|\partial\vec{q}\|} \tag{58}$$

This reduced quaternion then relates to the actual quaternion according to the following equation where the hat over the q represents the estimated quaternion and the symbol $\otimes$ represents quaternion multiplication (Sturm II, 2005):

$$q = \partial\vec{q} \otimes \hat{q} \tag{59}$$

Unfortunately, this author was unclear how the algorithm was supposed to contain both the estimated quaternion, which the algorithm should be finding, and the actual quaternion. Therefore, the Kalman Filter described hence forth does filter and predict the reduced state vector but does not convert that reduced state vector back into the full state vector.

Since the Kalman Filter requires a quaternion representation of the state, it is necessary to find the A and B matrices of Equation 6, repeated below for convenience, in the new representation. Equation 60 is the altered A matrix (Sturm II, 2005). B does not change since it was the right hand side of the equation which does not depend upon the representation.

$$\dot{x} = Ax + Bu \tag{6}$$

$$A = \begin{bmatrix} 0 & \omega_1 & -\omega_2 & .5 & 0 & 0 \\ -\omega_3 & 0 & \omega_1 & 0 & .5 & 0 \\ \omega_2 & -\omega_1 & 0 & 0 & 0 & .5 \\ 0 & 0 & 0 & 0 & \left(\frac{J_2 - J_3}{J_1}\right)\omega_3 & \left(\frac{J_2 - J_3}{J_1}\right)\omega_2 \\ 0 & 0 & 0 & \left(\frac{J_3 - J_1}{J_2}\right)\omega_3 & 0 & \left(\frac{J_3 - J_1}{J_2}\right)\omega_1 \\ 0 & 0 & 0 & \left(\frac{J_1 - J_2}{J_3}\right)\omega_2 & \left(\frac{J_1 - J_2}{J_3}\right)\omega_1 & 0 \end{bmatrix} \tag{60}$$

However, in the control algorithm section, u was defined based upon the Euler angles. It must now be represented by the new reduced state vector. Thus Equations 16, 21, and 22 are restated as Equations 61, 62, and 63 respectively:

$$u_2 = -2k_{p2}\partial q_2 - 2k_{d2}\partial\dot{q}_2 \tag{61}$$

$$u_1 = -2k_{p1}\partial q_1 - 2k_{d1}\partial\dot{q}_1 \tag{62}$$

$$u_3 = -2k_{p3}\partial q_3 - 2k_{d3}\partial\dot{q}_3 \tag{63}$$

It is important to note that the quaternions do not work like Euler Angles. The derivative of a term in a quaternion is not the attitude rate. However, the derivative of the reduced quaternion can be defined as follows:

$$\dot{\partial q} = .5\begin{bmatrix} 0 & \omega_3 & -\omega_2 & \omega_1 \\ -\omega_3 & 0 & \omega_1 & \omega_2 \\ \omega_2 & -\omega_1 & 0 & \omega_3 \\ -\omega_1 & -\omega_2 & -\omega_3 & 0 \end{bmatrix}\partial q - .5\partial q \otimes \begin{bmatrix} \omega_1 \\ \omega_2 \\ \omega_3 \\ 0 \end{bmatrix} \tag{64}$$

With these equations and terms defined, attention can now be turned to defining H_k, R, and Q. H_k is the observation matrix, which changes with each time step as the magnetic field changes. When using the reduced state representation, it is defined as follows (Sturm II, 2005), where the b vector is the magnetic field vector:

$$H_k = \begin{bmatrix} 0 & 2b_3 & 2b_2 & 0 & 0 & 0 \\ 2b_3 & 0 & 2b_1 & 0 & 0 & 0 \\ 2b_2 & 2b_1 & 0 & 0 & 0 & 0 \end{bmatrix} \tag{65}$$

R is the measurement noise matrix and is dependent upon the chosen magnetometer. It is defined in the following equation, where σ^2 is the square of the standard deviation of the magnetometer (Sturm II, 2005):

$$R = \sigma^2 \begin{bmatrix} 1 & 0 & 0 \\ 0 & 1 & 0 \\ 0 & 0 & 1 \end{bmatrix} \tag{66}$$

Q is the process noise matrix, defined by Equation 67. The m in front of the identity matrix is a value that will need to be set during filter tuning. Essentially, when the final system of the satellite is determined, the value of m should be varied until an optimal value is found. For questions about this sizing, please see the reference by Erick Sturm II.

$$Q = m \begin{bmatrix} 1 & 0 & 0 \\ 0 & 1 & 0 \\ 0 & 0 & 1 \end{bmatrix} \tag{67}$$

Now with all the variables defined, it would seem the filter should be able to run. However, attention must be turned to initialization of the system. It must be assumed that when the Kalman Filter first initializes, the satellite has no idea where it is or as it's often called is "lost in space". The satellite can take magnetometer readings but it must be able to initialize its guess for the attitude rates. This initialization is done according to the follow equation, where the vectors B_1 and B_2 are the first and second magnetic field vector in the body fixed frame (Sturm II, 2005):

$$\vec{\omega}_0 = \frac{\vec{B}_1 \times \frac{\vec{B}_2 - \vec{B}_3}{\Delta t}}{\left\|\vec{B}_1\right\|^2} \tag{68}$$

The other term to be initialized is the error covariance matrix. The initial guess will be of the form seen in Equation 69. However, like Q, this initial guess for P needs to be tuned for the final system (Sturm II, 2005).

$$P_0 = p \begin{bmatrix} 1 & 0 & 0 \\ 0 & 1 & 0 \\ 0 & 0 & 1 \end{bmatrix} \tag{69}$$

Thus ends the explanation of the Kalman Filter algorithm. A simulation should be run once the final system is defined so that tuning of the Q and P_0 can be done.

C. Fine ADCS

For a reaction wheel system it is fairly common to use the straightforward PD controller. Therefore, the same analysis done in the Coarse Control Law Development section Theoretical Torque holds true here. That is the theoretical torque is still calculated via Equations16, 21, and 22.

However, reaction wheels are not perfect systems any more than torque rods are. Reaction wheels have their own dynamics that limit the torque that can be applied to the system. Whereas torque rods are limited by their moment arm and the magnetic field of the Earth, reaction wheels are limited by the moment of inertia of the reaction wheel and the rotational acceleration, as can be seen in Equation 70, where I is the moment of inertia taken on the axis of rotation, $\ddot{\theta}$ is the rotational acceleration of the reaction wheel, and $\dot{\theta}$ is the rotational velocity.

$$u = I\ddot{\theta} + \omega \times I\dot{\theta} \tag{70}$$

Reaction wheels, as seen in the equation and discussed previously, produced torque by spinning a wheel. Unlike torque rods, the reaction wheel is a moving part within the spacecraft. The entire principle of these wheels producing torque is that their rotation causes the satellite to rotate in the opposite direction to conserve angular momentum. Because of this, it is not good enough to take the earlier derived equations of motion for this system. The rotation of these wheels must be taken into account in the system's equations of motion. These equations of motion are derived from the conversation of angular momentum, which is seen in Equation 71, where H is total angular momentum, J is the moment of inertia matrix for the spacecraft, J is the moment of inertia matrix for the reaction wheels, ω is the angular velocity vector of the spacecraft, and $\dot{\theta}$ is a vector comprised of the angular velocities of the reaction wheels.

$$H = J\omega + I\dot{\theta} \tag{71}$$

The derivative of angular momentum is torque, and if the derivate of Equation 71 is taken, Equation 72 is found.

$$J\dot{\omega} + \omega \times J\omega + I\ddot{\theta} + \omega \times I\dot{\theta} = 0 \tag{72}$$

This equation is the new equation of motion, where the first two terms characterize satellite behavior and the second two terms characterize the behavior of the reaction wheels, as predicted in Equation 70. These added

reaction wheel terms require an even more complicated simulation than created for the torque rod system, for the reaction wheel behavior must be captures and properly propagated.

Reaction wheels must also be on occasion desaturated, that is their momentum must be dumped. This must also be taken into account within the simulation.

D. Flight Rules

Flight rules are considerations that need to be taken into account in subsystem design even though the requirements do not directly dictate their existence. Both the coarse and fine ADCS have flight rules that need to be considered.

For the coarse ADCS system, it is important to recall that the attitude sensor being used in a magnetometer, which takes in magnetic field readings. These magnetic field readings are filtered in the Kalman Filter to determine the attitude; however, the filter is not robust enough to handle large magnetic pollution from the satellite. A torque rod creates a magnetic field in order to create torque. Such a magnetic field would pollute the magnetometer reading, affecting the attitude determination ability of the satellite. The current algorithm developed in the Control Law Development section of this paper assumes an almost continuous system where the torque rods can be run continuously. However, a Flight Rule for this system requires cycling between the magnetometer and torque rods, so that the magnetometer is either not on or its readings are disregarded while the torque rods are producing a magnetic field. This must be taken into account in the future work done on the torque rod system. Though the attitude can be propagated by the Kalman Filter while the torque rods are on, providing a practically continuous attitude knowledge update, a torque cannot be produced while a magnetometer reading is being taken. Therefore, the algorithm needs to take into account these periods of zero torque.

For the fine ADCS system, it must be taken into account that the reaction wheels will reach a point of momentum saturation. At this point, the reaction wheels will not be able to provide any more momentum to the satellite. When this happens, the torque rods must be engaged to desaturate the reaction wheels, dumping the excess momentum. This momentum saturation and subsequent desaturation must be taken into account as the algorithm for the fine ADCS system is developed. Therefore, the Flight Rule is that the reaction wheels must be desaturated using the torque rod system.

These two flight rules are the only current flight rules imposed upon the system; however, future flight rules can be developed as the designer sees fit.

VI. Conclusion

In conclusion, the purpose of this paper was to present the design of the attitude determination and control subsystem of the Prox-1 spacecraft as it is to this date. This included the requirements derivation, since any designer must have a firm understand of the requirements for the design of any subsystem. From these requirements, the architecture of the entire subsystem was discussed, including the need for a break down into fine and coarse systems. With the architecture known, hardware was selected using trade studies and tests for the hardware were developed. Then a detailed discussion and derivation of the coarse ADCS algorithms took place followed be a discussion of the fine system. Each of these parts is integral to an attitude determination and control subsystem, and though there is still work to be done in order to bring this subsystem to flight readiness, the discussions presented represent a solid foundation for the attitude determination and control subsystem of the Prox-1 satellite.

Acknowledgements

This paper would not have been possible without the help and support of numerous individuals. Firstly, the author would like to thank Luke Walker who initiated the study of the R^3 ADCS system and then became Project Manager of the R^3 team where he still played a vital role in supporting this subsystem. She would also like to thank Sarah McNeese the Project Systems Engineer and I&T Lead for the R^3 mission, whose assistance in developing the tests for the subsystem was invaluable. Of course, this paper would not have been possible without the various members of the R^3 and Prox-1 ADCS team: Thomas Fay, Mark Lieberbaum, Anand Nallathambi, Alexander Taleb, Lloyd Walker, and Kyle Yawn. The author would like to thank Charles Schira of Ball Aerospace, Paul Graven of Microcosm, Inc., and Josue Munoz of the Air Force Research Laboratory, who all took time out of their busy schedules to give advice and guidance to her. The author would like to particularly thank Nuno Filipe, without whom she would still be spinning her wheels on the most basic of concepts. She would also like to thank her parents for their continued support and guidance throughout her life. And of course, the author would like to thank Professor David Spencer, for serving as the Principle Investigator for the R^3 and Prox-1 missions as well as her research advisor and giving her the opportunity to lead the ADCS team.

References

Star Tracker ST: Manual of Operation. (2008, September 24). Valley Forge Composite Technologies, Inc.

Bate, R. R., Mueller, D. D., & White, J. E. (1971). *Fundamentals of Astrodynamics.* Mineola, NY: Dover Publications, Inc.

Comtech AeroAstro, Inc. (n.d.). *Coarse Sun Sensor Data Sheet.*

Hart, C. S. (2007). *Satellite Attiutde Determination using Magnetometer Data Only.* American Institute of Aeronautics and Astronautics.

Maus, S., Macmillan, S., McLean, S., Hamilton, B., Thomson, A., Nair, M., et al. (2010). *The US/UK World Magnetic Model for 2010-2015.* NOAA Technical Report NESDIS/NGDC.

Nise, N. S. (2004). *Control Systems Engineering.* Hoboken, NJ: John Wiley and Sons, Inc. .

Psiaki, M. L. (2000). Magnetic Torquer Attitude Control via Asymptotic Periodic Linear Quadratic Regulation. *AIAA.*

S.A. Lavochkin Scientific and Production Association. (2008). *The Star Tracker ST: Manual of Operations.*

SpaceQuest, Ltd. (n.d.). *ANT-GPS Specification Sheet.*

SpaceQuest, Ltd. (n.d.). *GPS-12-V1 Specification Sheet.*

SpaceQuest, Ltd. (n.d.). *MAG-3 Specification Sheet.*

Sturm II, E. J. (2005). *Magnetic Attitude Estimation of a Tumbling Spacecraft.* San Luis Obispo, CA: California Polytechnic State University.

Vallado, D. A. (2007). *Fundamentals of Astrodynamics and Applications.* Hawthorne, CA: Microcosm Press.

Welch, G., & Bishop, G. (2001). *An Introduction to the Kalman Filter.*

Wertz, J. R. (1978). *Spacecraft Attitude Determination and Control.* Dordrecht, Holland: D. Reidel Publishing Company.

Wertz, J. R., & Larson, W. J. (1999). *Space Mission Analysis and Design.* Hawthorne, CA: Microcosm Press, Inc.

Wie, B. (1998). *Space Vehicle Dynamics and Control.* Reston, Virginia: AIAA.

Appendix: Technical Memorandums

Magnetic Torque Rod Design Document
Author: Eric Van Gehuchten and Lloyd Walker
Date: 12/8/2010

Purpose

This document details the design and process of design for the magnetic torquer rod device for the Georgia Institute of Technology R^3 spacecraft. Current progress of the design and future plans of the implementation of this device are discussed.

Magnetic Torquers

When using reaction wheels for attitude control, saturation becomes a concern. Saturation happens when the reaction wheels build up stored momentum. This momentum must be canceled out for the reaction wheels to be effective. Magnetic torquers (often referred to as torque rods or magnetotorquers) will be used on the R^3 spacecraft to desaturate the reaction wheels as well as provide coarse attitude control. Three magnetic torquers will be placed orthogonally in the same direction as the reaction wheels. This will simplify control law creation as well as facilitate effective and efficient desaturation maneuvers.

Magnetic torquers operate very simply. A coil generates a magnetic moment. This moment acts against the Earth's magnetic field and creates a mechanical torque on the spacecraft. This mechanical torque is what will be used to turn the spacecraft and desaturate reaction wheels. (Sidi, 1997).

Because the operation of magnetic torquers is so simple, a simple calculation based on disturbance torquers and the Earth's magnetic field is utilized (Wertz & Larson, 2007). This calculation revealed that the magnetic torquers would need to provide a magnetic dipole of approximately 4 Am^2. For the sake of margin, a magnetic torquer with a dipole moment of 10 Am^2 was chosen.

To produce the required magnetic moment two types of magnetic torquers were considered: magnetic coils and torquer rods. Magnetic coils are large diameter coils of wire that utilize the internal area as the primary driver of magnetic moment. This device has the benefit of requiring fewer turns of wire; however, these coils are of a larger diameter and circumference. A magnetic torquer rod is a device with a small diameter and long length wound around a central core made of a magnetic material. This device uses the magnetic amplification properties of the core material to drive the magnetic moment.

For the level of magnetic moment needed by the R^3 spacecraft, magnetic coils become prohibitive in their mass and size. In the case of our 10 Am^2, the diameter of the coil would need to be nearly 70 centimeters, which is larger than the spacecraft, to supply the dipole moment. A torque rod of the same mass would remain within a two-centimeter diameter and 30 centimeter length. For this reason a set of torquer rods has been chosen as the method of magnetic torque control.

Initially, a commercial off the shelf magnetic torquer was considered. However, due to the simplicity of the device, it was decided that the torque rod would be developed and built in house. This design would be based off of the previously considered commercial model, the Microcosm Inc. MT10-2-H. This model would serve as the design basis with specifications as shown in Table XVIII.

Table XVIII Magnetic Torquer Rod Design Specifications

Magnetic Torquer Design Goals		
Dipole Moment	10	Am^2
Mass	0.35	kg
Length	330	mm
Diameter	17	mm
Power	1	W

The choice of core material is an important consideration in the design of a torquer rod. Several materials were considered for this purpose, but few offered affordable options in a rod form. The materials considered varied from simple materials, such as steel and exotic alloys like Hiperco 50. Additionally, a core of approximately one-centimeter diameter would best match the size of the intended device. To achieve our magnetic moment we also desired a material that would not saturate easily and have a high magnetic permeability. For these reasons Hiperco 50 alloy was chosen. It possesses a high permeability and can be available in rod form of comparable dimensions to our purpose. Further research on the Hiperco 50a shows that the metal needs to be annealed in order to achieve desired magnetic characteristics.

For the next step in the design process, the driving coil circuit was required. This coil would produce the magnetic field through the core, which would in turn provide the needed dipole moment. Using the finite element magnetic modeling program MagNet, the torque rod was modeled for several dimension choices and coil counts. This process was repeated until the model produced the desired magnetic moment. This resulted in a coil with approximately 7500 turns of wire, including a 10% margin to account for unforeseen problems arising from the computer modeling. This number of turns is currently being further refined to aid in possible mass savings.

The system wiring was determined by the electrical power system requirements provided. As the rod could require no more than one watt and would be operated at 12 volts, this limited the current to be 0.083 Amperes as determined by equation 1. This further determined the resistance of the system would be limited to 144 ohms using equation 2.

$$I = \frac{P}{V} \tag{1}$$

$$R = \frac{P}{I^2} = \frac{V^2}{P} \tag{2}$$

These two limitations required that the wire used to wrap the coil would be of a larger gauge than 32 American Wire Gauge. To save mass while allowing for a safety margin in the wire choice, 30-gauge wire was chosen. An increased wire size would also reduce power consumption of the device by up to two tenths of a watt. This wire would be connected via a two lead connector to the spacecraft systems for power.

With the two components of the torquer designed a mass estimate could be produced. With a known density of the core material and defined dimensions, the core mass was determined. For the wire windings, the total length of wire was determined. Using the circumference of the core and accounting for the increased diameter from stacked wiring layers, a total length of wire was estimated to be 274 meters. With a standard linear density of the designed magnet wire, mass was then calculated. The masses associated with the two components are shown in Table XIX along with a total component mass estimate.

Table XIX Magnetic Torquer Mass Estimate

Torquer Mass (kg)	
Solid Core	0.19
Wire windings	0.13
Subtotal	0.32
Contingency (15%)	0.05
Total Mass	0.36

Production

The materials needed in order to complete production of the magnetic torque rod were procured over the summer of 2010. Once received the Hiperco 50a cores were milled down to final dimensions and then sent off for annealing. When the torque cores were returned fabrication of the ground model started. This process was completed by modifying a solenoid lathe. The 30 gauge would be wrapped around the core approximately 8500 times building up 8 layers. The time duration for fabrication is around 6-8hrs.

Testing

In order to find out the magnetic dipole of the magnetic torque rods the magnetic field needed to be measured at different distances. The test would be replicate the procedures found in the 'On Determining Dipole Moments of a Magnetic Torquer Rod – Experiments and Discussions' in the Canadian Aeronautics and Space Journal Vol. 48. The torque rod was set to a current .0833 amps and with a gauss meter the magnetic field was measured 20, 30, 40, 50 and 60 centimeters from the center. The magnetic dipole was then calculated using formula 8 from the article.

Open Areas

The only remaining open area is the integration and testing with the control laws currently being developed. In this area, the housing design needs to be finalized, and the torque rod needs to be integrated with the flight computer.

Torque Rod Construction Memorandum
Author: Mark Liberbaum
Date: 12/15/2010

Materials used:

1 Hiperco 50a metal alloy rod—0.5" in diameter, 12" long

2 Stainless Steel Washers, 0.75" in diameter, 1 millimeter thick

450 Meters of enamel coated 30 gauge copper wire

Procedure to build a torque rod:

First, the rods were bought. The rods were purchased for approximately $400 dollars per rod from Eagle Alloys, located at:

Eagle Alloys Corporation
178 West Park Court
Talbott, TN 37877-8674
(423) 586-8738

The alloy they are made of is Hiperco 50a. The composition of Hiperco 50a follows.

Table XX Composition of Hiperco 50a alloy

0.05%	Silicon
2.00%	Vanadium
0.05%	Manganese
48.75%	Cobalt
49.15%	Iron

This alloy is unique because when annealed properly, it has a very high magnetic permeability, thus making it ideal to produce a strong magnetic flux density and therefore a strong magnetic dipole moment.

First, the core was taken to the machine shop. The raw rod was greater than 0.5" in diameter; thus, we asked the machine shop to trim it down to a diameter of 0.5". Then we had the machine shop weld the two stainless steel washers to the core, 0.5 cm (0.1969 in) from each end. A drawing of the core is shown below:

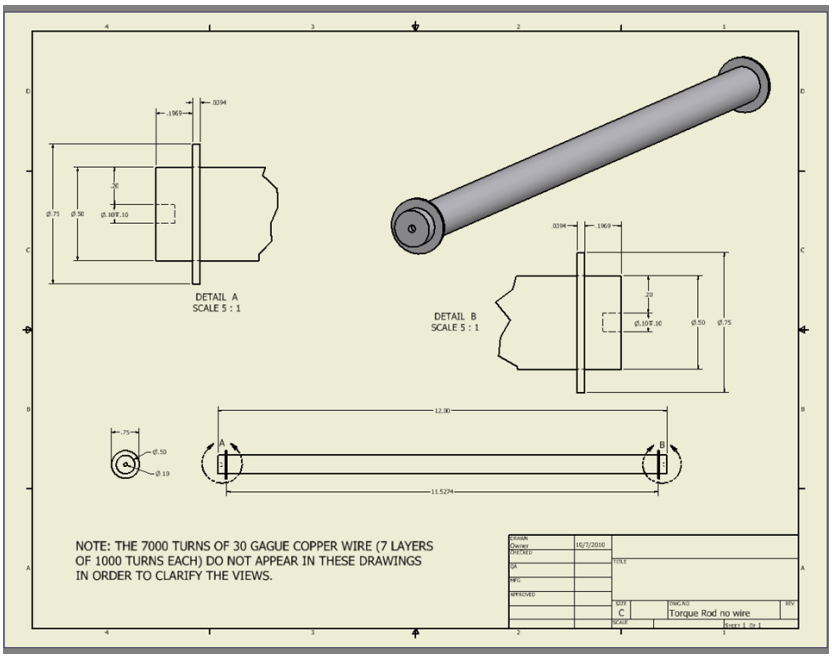

Figure 11 Drawing of the Torque Rod Core

Next, the core had to be annealed, or heat treated. This was to align the molecules in the core to produce the desired properties. The core was annealed at:

Braddock Heat Treating Co Inc

123 Chimney Rock Road

Bridgewater Township, NJ 08807-3126

(732) 356-2906

When the cores arrived back, it was time to wrap the wire. To wrap approximately 9,000 turns by hand, we used a special solenoid machine at the High Power Electric Propulsion Laboratory. This was the trickiest part; the wraps of wire had to be flush, and any gap in the beginning was greatly magnified in the layers above it.

To start, the right plate of the machine was moved to the right, and the core was inserted. To insert the core, a small metal plate was used: one side had two parallel slit-like cuts; the other side had a circular cut. The side with the slit-like cuts went against the motor; and the core was inserted into the circular cut on the other side. The other end of the core (nearest to the right plate of the machine) was put in a washer, to avoid friction of the metal of the core wearing down the hole in the right plate. The right plate was then screwed back in, so that the core was held nice and tight against the motor. To ensure that the plate was perpendicular to the floor and it was tight

enough, the motor was run for a few turns. Little to no up and down motion meant that the plate had been screwed on successfully.

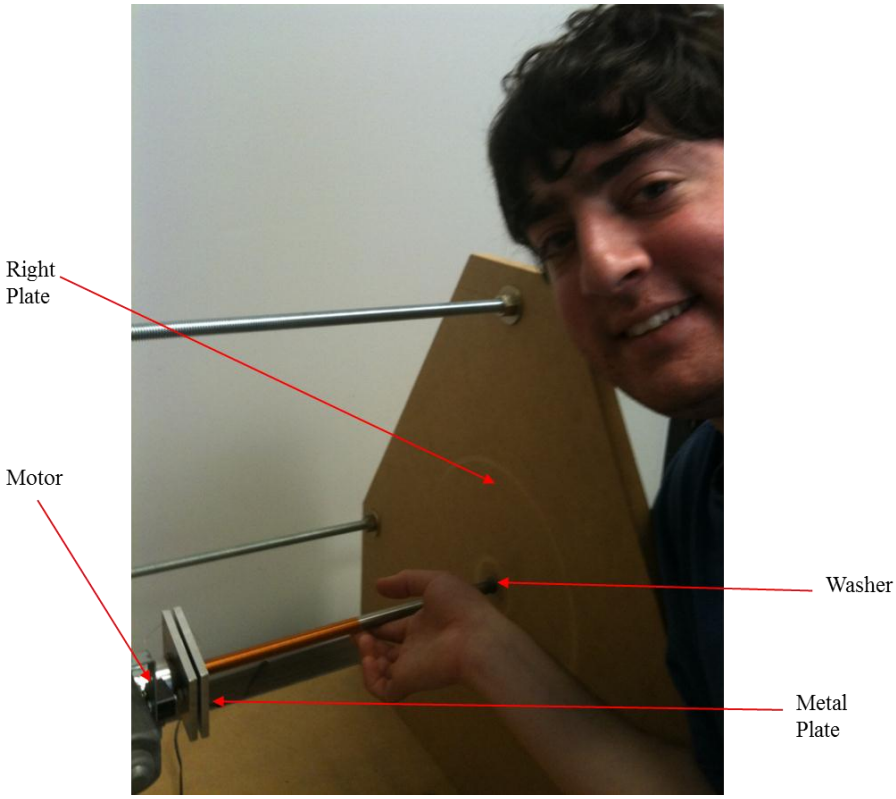

Figure 12 Torque Rod Machining Device

To control the motor, two foot petals were used. One rotated the structure (metal plate and core) in a direction that allowed the wrapping of wire, and one reversed it (to unwrap in case a mistake was made). To begin wrapping, approximately 6 inches of wire was left on the outside (to attach the wire to a circuit, etc.). Getting the wrapping started was difficult; in fact, the first few turns involved turning the structure once, and shifting the wire over by hand. Once the wire was started, however, the wrapping became much easier. This was a two person job; one person was at the machine, and the other person was sitting behind the first person, with the spool of wire on a screwdriver, letting it feed to the machine. The voltage applied to the motor (which controlled the motor speed) was anywhere between 3 volts at the beginning to 11 volts.

Several techniques were found to make the process easier. First, the machinist would hold his or her finger in a position approximately 6 inches under the core, and let the copper wire wrap around his or her finger 90 degrees from the wire spool holder to the torque rod. The friction between the machinist's hand and the copper wire provided sufficient tension in the wire; too little tension and too much tension were undesirable. The machinist's

other hand went on top of the torque rod: the machinist used his or her fingernail to push against the wire as it was being wrapped on the core. Not only did this create a nice flush layer of wire, but it also allowed for self correcting—with any small gaps that were inevitably created, the machinist simply had to apply more pressure with his or her fingernail, and the gap would go away in 4 or 5 turns. Furthermore, it was found that doing the last 50 or so turns by hand (with the core off of the machine) was much easier than doing it on the machine.

Eight layers were created. This amounted to approximately 9000 turns. After the eighth layer was complete, the wire was cut, again leaving approximately 6 inches of unwrapped wire to connect the torque rod to a circuit. Thus, the torque rod was built.